이학박사 학위논문

In vivo imaging of ^{64}Cu-HSA-aptamer as a targeting agent for HER2 (Human Epidermal Growth Factor Receptor 2) expressing cancer cells

방사성구리-알부민-앱타머를 이용한 HER2 표적 암세포 생체영상

2014 년 8 월

서울대학교 대학원
종양생물학 협동과정

송 명 근

A thesis of the Degree of Doctor of Philosophy

방사성구리-알부민-앱타머를 이용한 HER2 암표적 생체영상

In vivo imaging of ^{64}Cu-HSA-aptamer as a targeting agent for HER2 (Human Epidermal Growth Factor Receptor 2) expressing cancer cells

August 2014

Myung Geun Song

Interdisciplinary Program in Tumor Biology
Seoul National University College of Medicine

ABSTRACT

Myung Geun Song

Interdisciplinary Program in Tumor Biology

The Graduate School

Seoul National University

Objective: Human epidermal growth factor receptor-2 (HER2) is one of the most important cancer biomarkers. It has been reported that HER2 overexpression in breast cancer patients correlates with a poor prognosis and resistance to therapy. A humanized HER2 monoclonal antibody, trastuzumab (Herceptin), has been used for HER2-targeted imaging and therapy. However, immunosintigraphy showed a relatively low target-to-background ratio, which induced low detectability. Therefore, there is a need for a new imaging probe to detect HER2 expression *in vivo*. To develop a new imaging probe using aptamer, single-stranded DNA or RNA oligonucleotides, ^{64}Cu-labeled human serum albumin (HSA) with HER2-specific aptamer was designed and *in vitro* and *in vivo* properties of targeting HER2 expressing cancer cells were evaluated.

Methods: HER2-targeted aptamer was developed using systematic evolution of ligands by exponential enrichment technology (SELEX) and the aptamer was conjugated with human serum albumin (HSA) for prolonged blood circulation. FITC-

labeled aptamer was used for confocal microscopy to monitor *in vitro* targeting. HSA was consecutively conjugated with SCN-*Bn*-NOTA and the bifunctional cross-linker sulfo-SMCC, which was then covalently conjugated with HER2-specific aptamer. The resulting NOTA-HSA-aptamer was further radiolabeled with $^{64}CuCl_2$. Labeling efficiencies and purity of ^{64}Cu-HSA-aptamer were determined by instant thin layer chromatography (ITLC). For *in vivo* tumor imaging, ^{64}Cu-HER2 aptamer and ^{64}Cu-HSA-HER2 aptamer were intravenously injected to MDA-MB468 and KPL4 tumor-bearing nude mice and their uptakes were imaged by PET from 0 to 46 h. The biodistribution of ^{64}Cu-HER2 aptamer and ^{64}Cu-HSA-HER2 aptamer was examined in KPL4 and MDA-MB468 human breast tumor-bearing mice at 1 and 22 h post-injection. Autoradiography was performed to compare radiouptake between ^{64}Cu-HER2 aptamer and ^{64}Cu-HSA-HER2 aptamer in tumor tissues.

Results: FITC-HER2 aptamer uptakes were visualized by confocal microscopy in HER2-positive cells (T47D and KPL4 cells), but not in HER2-negative cells (MCF7 and MDA-MB468 cells). Purity of both ^{68}Ga-HER2 aptamer and ^{64}Cu-HSA-HER2 aptamer was over 95% and *in vitro* uptake test showed their specific binding to HER2 in KPL4 cells (up to 3-fold increase). In KPL4 cells, the 50% inhibitory concentration (IC50) values for the HSA-aptamer, NOTA-aptamer and aptamer-biotin were estimated to be 1.44 ± 0.23, 12.97 ± 0.23 and 9.68 ± 0.26 nM, respectively. ^{68}Ga-HER2 aptamer was quickly excreted in the urine or hepatic pathway within 46 h after tail vein injection. However, HSA conjugated HER2 aptamer was excreted slowly in

the urine compared to HER2 aptamer. In tumor tissues, radio uptake of ^{64}Cu-HSA-HER2 aptamer was increased compared to HER2 aptamer. Serial PET imaging revealed that KPL4 tumor uptake of ^{64}Cu-HSA-HER2 aptamer was 1.67 ± 0.15, 4.63 ± 2.66, 5.72 ± 3.22 and 6.63 ± 1.22 %ID/g at 5 min, 10, 22, and 46 h post-injection, respectively. In KPL4 tumor, ^{64}Cu-HSA-HER2 aptamer biodistribution were also examined to be over 4.74 ± 1.60 and 8.98 ± 0.19 %ID/g at 1 and 22 h post-injection respectively, which was about 3.4-fold higher than that of ^{64}Cu-HER2 aptamer. Moreover, the KPL4 tumor uptake of ^{64}Cu-HSA-HER2 aptamer was about 4.2-fold higher than the MDA-MB468 tumor uptake. Autoradiograms revealed accumulation of HSA-HER2 aptamer in HER2-positive tumor tissues. The localizations of HSA-HER2 aptamer-FITC in KPL4 tumor indeed corresponded to the distribution of the HER2-positive cells.

Conclusion: Tumor uptake of HSA-conjugated aptamer was increased compared to HER2 aptamer. ^{64}Cu-HSA modified aptamer could be a promising probe for HER2-specific molecular imaging. The strategy using HSA as a carrier to prolong blood circulation of biomolecules such as aptamer could be applied in the design of many other radiolabeled probes and radionuclide therapy agents.

Keywords: Human Epidermal Growth Factor Receptor 2 (HER2), Aptamer, Human serum albumin (HSA), PET imaging, ^{64}Cu, Targeted therapy

Student number: 2010-30593

LIST OF FIGURES

LIST OF ABBREVIATIONS

HER2	**:**	**Human Epidermal Growth Factor Receptor 2**
SELEX	**:**	**Systematic Evolution of Ligands by Exponential Enrichment**
HSA	**:**	**Human Serum Albumin**
FBS	**:**	**Fetal Bovine Serum**
FITC	**:**	**Fluorescein Isothiocyanate**
^{68}Ga	**:**	**Gallium-68**
^{64}Cu	**:**	**Copper-64**
DOTA	**:**	**1,4,7,10-tetraazacyclododecane-1,4,7,10-tetraacetic acid**
NOTA	**:**	**1,4,7-triaza-cyclononane-1,4,7-triacetic acid**
ITLC-SG	**:**	**Instant Thin Layer Chromatography-Silica Gel**
PET	**:**	**Positron Emission Tomography**
%ID/g	**:**	**% Injected Dose/tissue gram**
IC50	**:**	**50% inhibitory concentration**

CONTENTS

INTRODUCTION

HER2 as a cancer biomarker

Human epidermal growth factor receptor 2 (HER2), a tyrosine kinase receptor which belongs to the epidermal growth factor receptor (EGFR/HER1) family (1) is frequently overexpressed in a wide range of human tumors including breast, ovarian, lung, and gastric cancers (2-4). Molecular-targeted imaging and therapy of various types of cancers have been developed. Approximately 20-30% of invasive breast carcinomas overexpressed human epidermal growth factor receptor 2 (HER2), and HER2-positive breast cancer is associated with more malignant behaviors, including increased invasiveness, higher recurrence, and reduced overall survival rate (5-13), comparing to other types of breast cancer. Therefore, targeting of the receptor is thought to be beneficial for cancer patients with HER2 amplification. Moreover, more than half of the HER2-positive women are estrogen receptor(ER)/progesterone receptor(PR)-negative, suggesting that a fair proportion of HER2-positive breast cancers do not respond well to endocrine therapies (14-16). For those patients only accepting the conventional treatments of surgical resection followed by chemo- and endocrine therapies, the median survival time of HER2-positive patients was about half of that of HER2-negative cases (16, 17). In view of the above situation, the development of novel therapy for HER2-positive breast cancer, such as tumor-targeted therapy, is an inevitable trend.

Targeted treatment of HER2-positive breast cancer

Targeted therapy is characterized by selective killing of tumor cells with minimal influence to normal cells, and may improve therapeutic efficacy and reduce adverse effect. HER2 overexpression predicts response to trastuzumab (Herceptin), a humanized HER2 monoclonal antibody directed against the HER2 extracellular domain (18), which has been approved as a first line targeted treatment of HER2-positive metastatic breast cancer. And lapatinib, a small tyrosine kinase inhibitor (TKI) which simultaneously inhibits the activity of EGFR and HER2 (19). These two agents have shown to improve remarkably the clinical outcome of patients with tumors carrying HER2 abnormalities.

However, drug resistance is developed rapidly with trastuzumab treatment in virtually all patients (6, 7, 20-23). Currently, there are no standard approaches in the management of HER2 positive patients developing resistance to trastuzumab and lapatinib. Great efforts are focused at finding new targeting agents or strategies to prevent or overcome resistance in HER2-overexpressing cancer cells. Based on preclinical rationale, much of these efforts focus on the exploitation of HER2 either by using pan-HER inhibitors, monoclonal antibodies that inhibit the formation of heterodimers within the EGFR family, combinations of drugs to simultaneously inhibit HER2 and other relevant targets as the mammalian target of rapamycin (mTOR), or the Heat Shock Protein (HSP90) (24). However, usually, anti-tumor activity rates in these trials are low, in the range of 5–25% (25-27). Therefore, it is necessary to develop novel targeting therapeutic strategies for treatment of HER2-

positive breast cancer.

Aptamer for targeting agents

Tumor-targeted therapy requires ligands that can bind to cancer cells. In addition to antibodies, other types of novel tumor-targeting ligands have emerged in the past decades (28). Several ligands, like the antibody and aptamer, are actively used for targeting drug delivery systems. Among them, the aptamer has been issued as a powerful biological ligand because of its high selectivity and binding strength to the target molecules (29-31). Aptamers are single-stranded DNA or RNA oligonucleotides, which are selected in an evolutionary process called systematic evolution of ligands by exponential enrichment (SELEX). Selected sequences can be modified after selection to improve their stability in different chemical environments (e.g., serum). Aptamers are fold into specific 3D structures, which are comparable to antibodies in specificity and affinity for their target molecule, typically a protein (32, 33). Various aptamers have been developed against a variety of cancer targets, including intracellular, extracellular ligands and cell surface proteins (28). Aptamers have some advantages over an antibody, such as chemical synthesis *in vitro*, economical production, readily availability, easy modification, and high stability in various physical and chemical environments. At 8–15 kDa, aptamers are intermediate in size between antibodies (150 kDa) and small peptides (1–5 kDa) and are slightly smaller than single-chain, variable-fragment antibodies (scFvs, 25 kDa). Based on these advantages aptamers have shown great potential for novel targeted diagnostic and therapeutic applications (28, 34, 35). The first aptamer drug, Macugen, was approved for clinical use years ago. Other aptamer-based agents are being actively tested in clinical trials (36, 37).

So far, several anti-HER (EGFR)-specific aptamers have been developed (38-42). They generally show high affinity and specificity to their targets and, in the case of HER1- and HER3-specific aptamers, they also inhibit the proliferation of cultured cancer cells (38, 42). Notably, an aptamer against HER1 was able to inhibit tumor growth in a mouse model (40), and HER2-specific aptamers were used to deliver siRNAs targeting B-cell lymphoma 2 (Bcl-2) (43). Aptamers also can effectively deliver cytotoxic agents or radionuclides to the targeted tissue or organ (28, 34, 35). Radiolabeled aptamers are suitable for imaging applications due to their polyanionic nature and their small size and molecular weight (8−15 kDa), which are key properties leading to good tumor penetration, rapid tissue uptake, and rapid blood clearance. However, the fast systemic clearance is not an ideal characteristic when designing aptamer based therapeutics. Therefore, to overcome aptamer limitations such as fast clearance *in vivo*, it can be coupled to diagnostic or therapeutic agents and to bioconjugates, such as polyethylene glycol (PEG) polymers, metal-based nanoparticles and degradable particles, which can alter aptamer pharmacokinetics (44-47).

HSA as a carrier

Human serum albumin (HSA) is a 65 kDa protein that is abundant in the circulation and features low immunogenicity, high biocompatibility, and excellent biodegradability. Because of its long circulation property, it has been used as a carrier for drug delivery in advanced clinical trials (48). The renal filtration of these HSA-drug bioconjugates is also substantially inhibited by the high molecular size of albumin, thereby enabling prolonged exposure of the target cells to the bioconjugates.

In another study, integrin $\alpha_v\beta_3$-binding RGD peptide was conjugated with HSA to improve molecular probe pharmacokinetics and to prolong the probe circulation and tumor contrast (49). The resulting aptamer-albumin conjugates are expected to display several unique properties such as 1) improved pharmacokinetics in terms of a low renal accumulation due to the high molecular size of the conjugate, 2) improved tumor targeting ability because of the multimeric structure of the conjugate using aptamer ligands, and 3) improved blood circulation and tumor accumulation.

PET imaging with ^{64}Cu

Commonly used PET isotopes for antibody labeling include ^{64}Cu ($t_{1/2}$ = 12.7 h), ^{86}Y ($t_{1/2}$ = 14.7 h), ^{89}Zr ($t_{1/2}$ = 3.3 d), ^{124}I ($t_{1/2}$ = 4.2 d), among others (50). Currently, ^{64}Cu is the most widely used isotope for immunoPET, partly due to its wide availability, low cost, and versatile chemistry. The E_{max} of 656 keV for its positron emission, which is comparable to that of ^{18}F and lower than that of ^{124}I, can produce PET images with good spatial resolution. In addition, there are several radioisotopes of Cu available, which allow for both diagnostic imaging (with $^{60/61/62/64}$Cu) and therapeutic applications (with $^{64/67}$Cu) (51).

One of the key requirements for accurate PET imaging with ^{64}Cu-labeled probes is that the tracer should be sufficiently stable during the imaging period, since PET scanners detect the distribution of ^{64}Cu instead of the probes itself. Over the years, many bifunctional chelators have been investigated for ^{64}Cu labeling, such as 1,4,7,10-tetraazacyclododecane-1,4,7,10-tetraacetic acid (DOTA) (52, 53), 1,4,7-triaza-

cyclononane-1,4,7-triacetic acid (NOTA) (54-57), 1,4,8,11-tetraazacyclotetradecane-1,4,8,11-tetraacetic acid (TETA) (58), 1,4,8,11-tetraazacyclotetradecane-N,N′,N″,N‴-tetraacetic acid (BAT) (59), 4,11-bis(carboxymethyl)-1,4,8,11-tetraaza-bicyclo[6.6.2]hexadecane (CB-TE2A) (60, 61), 1,8-diamino-3,6,10,13,16,19-hexaaza-bicyclo[6,6,6]eicosane (Diamsar) (62, 63), among many others (50, 64).

Purpose of this study

HER2 overexpression in breast cancer patients has been reported to have correlation with a poor prognosis and resistance to therapy. A humanized HER2 monoclonal antibody, trastuzumab (Herceptin), has been the main approach for HER2-targeted imaging and therapy. However, drug resistance is commonly and rapidly developed with trastuzumab treatment. Therefore, there is a need for a new imaging probe to recognize HER2 protein *in vivo*. Here I wondered whether conjugation of a short-lived aptamer and albumin could improve its HER2 targeting property compared to original aptamer. ^{64}Cu labeled human serum albumin (HSA) with HER2-specific aptamer was designed. The biologic profiles of the resulting probe (^{64}Cu-HSA-aptamer) were studied to evaluate whether albumin-aptamer conjugates could increase the *in vivo* half-life and targeting efficiency in breast cancer cells with a high expression of HER2 and in nude mice bearing subcutaneous tumors.

MATERIALS AND METHODS

Cell culture

Human breast cancer cell line, MCF7, MDA-MB468, MDA-MB231, T47D and KPL4 were cultured in DMEM medium (Welgene, Daegu, South Korea) containing 10% (v/v) fetal bovine serum (FBS, Invitrogen, Grand Island, NY, USA) and 1% antibiotics (Invitrogen, Grand Island, NY, USA). Cell lines were incubated in a 37℃ humidified incubator with 5% CO_2 atmosphere.

Western blotting

Total proteins from cells (MCF7, MDA-MB468, T47D and KPL4) were isolated using RIPA buffer (25 mM Tris-HCl at pH 7.5, 2 mM EDTA at pH 8.0, 150 mM NaCl, 0.5% NP-40) and protease inhibitor (Roche, Nutley, NJ, Switzerland). Total proteins were measured using BCA protein assay kit (Pierce Endogen, Rockford, IL, USA). Lysate of each cell sample was loaded onto NuPAGE 4-12% Bis-Tris Gel (Invitrogen, Carlsbad, CA, USA). After electrophoresis, the gels were blotted onto PVDF membranes (Millipore, Watford, UK). The PVDF membranes were subjected to blocking with 3% skim milk in Tris-Buffered Saline Tween-20 buffer (20 mM Tris, 137 mM NaCl and 0.1% Tween 20) for 1 h at room temperature. The membranes were incubated overnight at 4℃ with primary antibody for Her2 (#2165, Cell Signalling Technology, Danvers, MA, USA) or β-actin (#A5441, Sigma-Aldrich, St.

Louis, MO, USA). Membranes were then probed with anti-rabbit or anti-mouse IgG (Cell Signalling Technology, Danvers, MA, USA). Visualization was performed using ECL reagents (Roche, Nutley, NJ, USA).

Aptamers

HER2 aptamer (5′-AGCCGCGAGGGGAGGGAUAGGGUAGGGCGCG GCU-3′) and scrambled aptamer (5′-GGAGAUGCUCCGGGCGGAGGCCGGGGG UAAAGGG-3′) were synthesized by ST Pharm Co. (Ansan, South Korea). For protection against nucleases, the aptamers contains 2′-fluoro cytocine and guanine (65, 66). The synthetic aptamers were produced with FITC dye (5′ end) and amine or thiol (3′ end) to serve as a HSA conjugation site.

Confocal microscopy

For immunofluorescence analysis in cancer cells, 1×10^5 cells (MCF7, MDA-MB468, T47D and KPL4) were seeded in each well of 12-well plate and fixed with 4% paraformaldehyde for 15 min and permeabilized in PBS containing 0.5% Triton X-100 for 5 min. The cells were blocked for 30 min with 10% BSA/PBS and washed three times with PBS. Cells were incubated with FITC-labeled scrambled or HER2 aptamer (10 nM or 50 nM) for 1 h. Cells were washed three times with PBS. After staining, the slides were mounted with Prolong Gold reagent (Invitrogen, Grand

Island, NY, USA). Fluorescence images were taken by confocal microscopy imaging system (Olympus IX81, Troy, NY, USA).

For immunofluorescence analysis in non-fixed cancer cells, each breast cancer cells (MCF7, MDA-MB468, T47D and KPL4) were seeded in a coverslip bottom 8-well chamber slide (Nalge NUNC International, Naperville, IL, USA) and overnight incubation. Attached cells were treated with 100 nM of Cy5.5-HER2 aptamer for 30 min and washed three times with PBS. Serial fluorescence images were taken by confocal microscopy imaging system (Olympus IX81, Troy, NY, USA) at 30 min and 6 h after the aptamer treatment.

For co-culture with HER2 negative cells and HER2 positive cells, MCF7 and MDA-MB468 cells were stained with the fluorescence cell tracker CM-DiI (Invitrogen, MO, USA) for 20 min and washed three times with PBS. Stained cells were seeded in a coverslip bottom 8-well chamber slide (Nalge NUNC International, Naperville, IL, USA) and then HER2 positive cells were added into the wells of HER2 negative cells. After 18 h incubation, cells were incubated with FITC-labeled HER2 aptamer (50 nM) for 1 h. cells were washed three times with PBS. The fluorescence images were acquired by confocal microscopy imaging system (Olympus IX81, Troy, NY, USA).

Bioconjugation of HSA with NOTA and aptamers

First, HSA (5 mg) was conjugated with SCN-*Bn*-NOTA (3.8 mg) in 200 μL of borate buffer (50 mM, pH 8.5) in a molar ratio of 1:100 for overnight at 4℃. The

resulting HSA-NOTA conjugate was then purified using a PD-10 column (GE Healthcare) and eluted with the same borate buffer. The fractions containing NOTA-HSA were concentrated using concentrator columns (Millipore, 50K MWCO, 1.5 mL) to a total volume of 50 μL. The purified NOTA-HSA was then reacted with 1 mg of sulfo-SMCC in molar ratio of 1:5 and in a total volume of 200 μL for 1h at 4℃. The resulting bioconjugate was further purified using the PD-10 column and phosphate-buffered saline (PBS, pH 7.4) as the eluent. Finally, aptamers were site-specifically conjugated to the NOTA and sulfo-SMCC modified HSA via the cysteine residue. The reaction was performed in a molar ratio of 1:5 using 200 μg of NOTA-HSA-SMCC and 50 μg of aptamer in a total volume of 300 μL for overnight at 4℃. The resulting bioconjugate, NOTA-HSA-aptamer, was then purified and concentrated through a microcentrifuge tube (Millipore, 50 kDa, 1.5 mL) to a final volume of 20 μL. After each step, the protein concentration was measured by the bicinchoninic acid (BCA) assay (Pierce), and the samples were analyzed via sodium dodecyl sulfate polyacrylamide gel electrophoresis (SDS-PAGE).

Radiolabeling of NOTA-aptamer and NOTA-HSA-aptamer

$^{68}GaCl_3$ in 0.1 N HCl was obtained from elution of ^{68}Ga generator (Eckert & Ziegler, Berlin, Germany). NOTA-aptamers (20 μg in 20 μL RNase free water) were mixed with 1 mCi / 0.2 mL $^{68}GaCl_3$ and the pH was adjusted to 6 using 0.5 M phosphate buffer. The reaction mixture was incubated at 95℃ for 30 min in heating

block. The mixture was purified by a PD-10 column (GE Healthcare), eluted with saline. The fractions were washed and concentrated using concentrator columns (Millipore, 10K MWCO, 1.5 mL) to a total volume of 25 μL. The labeling efficiency of NOTA-aptamer with ^{68}Ga was determined using Instant Thin Layer Chromatography (ITLC-SG) in 0.1 M citric acid. The strip was counted by Bio-Scan AR-2000 System imaging scanner (Bio-Scan Inc., Washington D.C, USA).

Approximately 400 μg of the NOTA-HSA-aptamer was radiolabeled with ^{64}Cu by addition of 37 MBq (1 mCi) of $^{64}CuCl_2$ in 0.1 N sodium acetate buffer (NaOAc, pH 6.5) and incubated for 1 h at 37℃. The radiolabeled complex was purified by a PD-10 column (GE Healthcare), eluted with saline, and passed through a 0.22 μm Millipore filter for both *in vitro* cell uptake studies and animal experiments. Radiolabeling of NOTA-HSA with ^{64}Cu was performed in the same way as for NOTA-HSA-aptamer.

In vitro cell uptake assays

The MDA-MB468 or KPL4 cells (3×10^5 or $10 - 0.156 \times 10^6$ as 1:2 serial dilution) were seeded per well in 5 mL test tubes and cells were washed once with serum-free DMEM medium and incubated with the probes (2 μCi per well, 2 μg) in 200 μL of serum-free DMEM medium at 37℃. Tubes of 3×10^5 cells were incubated with probes for 0.5, 1, and 2 h. And serial diluted cells were treated for 1 h. The cells were washed three times with cold PBS and lysed in 200 μL of 0.2M NaOH. The radioactivity of the cells was counted using a PerkinElmer 1470 automatic γ-counter.

The uptake (counts/min) was expressed as the percentage of added radioactivity.

Animal modeling and PET imaging

All animal studies were performed under approval from the Seoul National University Institutional Animal Care and Use Committee (IACUC). BALB/c nude mice (6 week old, female) were purchased from the Orient Bio Inc., (Seongnam, South Korea). Breast cancer cell lines were subcutaneously injected into left upper flanks (MDA-MB468, 5 x 10^6 cells) and right upper flanks (KPL4, 5 x 10^6 cells). Tumors were allowed to grow to a size of 0.5 - 0.7 cm in diameter (3 - 4 weeks). The tumor-bearing mice were subjected to *in vivo* biodistribution and imaging studies.

Small animal PET of tumor-bearing mice (n = 3 for each group) was performed using PET box (SOFIE Bioscience, Culver, CA, USA). Mice bearing MDA-MB468 and KPL4 tumors were injected with 1.5-1.9 MBq (40-50 μCi, 50-60 μg) of ^{64}Cu-HSA-HER2 aptamer via the tail vein. At various times after injection (1, 10, 22, and 46 h), the mice were anesthetized with 2% isoflurane and placed in the prone position. Static scans (for 1, 10, and 22 h, 10-min scans; for 46 h, 20-min scans) were obtained, and the images were reconstructed by AMIDE algorithm. As a control experiment, mice bearing MDA-MB468 and KPL4 tumors were injected with ^{64}Cu-HSA or ^{64}Cu-HSA-scrambled aptmaer (each 1.5-1.9 MBq, 40-50 μCi, 40-50 μg) via the tail vein. PET images were obtained by the same approach as for ^{64}Cu-HSA-HER2 aptamer).

Biodistribution Studies

For biodistribution studies, mice bearing MDA-MB468 and KPL4 xenografts (n = 3 for each group) were injected with 0.37 - 0.555 MBq (10 - 15 μCi, 15 - 20 μg) of ^{64}Cu-HSA-HER2 aptamer or ^{64}Cu-HER2 aptamer through the tail vein and sacrificed at different time points (1 and 22 h) post-injection (p.i.). To test the HER2-targeting specificity of ^{64}Cu-HSA-HER2 aptamer or ^{64}Cu-HER2 aptamer *in vivo*, MDA-MB468 and KPL4 tumor bearing mice were injected with a mixture of the radiolabeled probe and unlabeled probe (NOTA-HSA-HER2 aptamer, 500 ug; NOTA-HER2 aptamer, 100 ug). Tumor and normal tissues were excised and weighed, and their radioactivity was measured using a γ-counter. The radioactivity uptake in the tumor and normal tissues was expressed as a %ID/g.

Immunofluorescence analysis in tumor tissues

For immunofluorescence analysis in tumor tissues, the tumors were embedded within OCT compound and frozen for serial coronal sections with 5 μm thick on slides. Tumor sections were washed with 0.5% H_2O_2 in MeOH for 30 min and permeabilized in PBS containing 0.5% Triton X-100 for 5 min. Sections were then washed three times with PBS and incubated in normal horse serum (30:1 ratio) for 1 h at room temperature. The slides were incubated overnight with HER2 antibody (Cell Signalling Technology, Danvers, MA, USA) overnight. After staining, the slides were mounted with Prolong Gold reagent (Invitrogen, Grand Island, NY, USA). Fluorescence was observed using Zeiss LSM 510 META confocal imaging system

(Carl Zeiss, Jena, Germany).

Autoradiography

Mice bearing MDA-MB468 and KPL4 xenografts were injected intravenously with 1.5-1.9 MBq (40-50 μCi, 50-60 μg) of ^{64}Cu-HSA-HER2 aptamer or ^{64}Cu-HER2 aptamer. Twenty-two hours after injection, the animals were sacrificed and tumors excised, embedded in mounting medium (O.C.T. Compound; Sakura Finetek), and frozen. Sets of contiguous frozen tissue sections were cut at a 20 μm thickness on a Microm HM500 cryostat microtome (Microm International GmbH) and collected on glass microscope slides. Digital autoradiography was then performed on tissue sections. Sections were placed in a film cassette against a phosphor imaging plate (Fujifilm BAS-MS2325; Fuji Photo Film). Phosphor plates were read out at a resolution of 50 · 50 mm on a BAS-1800II Bio-Imaging Analyzer (Fujifilm Medical Systems).

RESULTS

Expression of Human Epidermal Growth Factor Receptor 2 (HER2) in breast cancer cell lines

To select a HER2 positive cell lines known to overexpress HER2 and bearing HER2 gene amplification, western blotting analysis confirmed a high-level expression of HER2. In the breast carcinoma lines MCF7, MDA-MB468, T47D and KPL4, analysis of HER2 cell surface expression revealed higher abundance in KPL4 cells and weak expression in T47D cells compared with MDA-MB468 and MCF7 (15.3-fold increase; Fig. 1).

In vitro imaging of HER2 using FITC-HER2 aptamer

In comparison to antibody, aptamers present several advantages for imaging: high affinity and specificity, smaller size for a better tissue penetration, and easy incorporation of chemical modifications (29-31). HER2 aptamer was conjugated with both FITC for fluorescence imaging and amine or thiol group for nuclear imaging (Fig. 2). The levels of expression of HER2 in the four cell lines were observed with confocal microscopy. As shown in Figure 3A, FITC signals were found in both the plasma membrane and cytosolic portion of HER2 positive T47D and KPL4 cells. Furthermore, as the concentration of HER2 aptamer in a media increased, fluorescence signals specifically increased in HER2 positive KPL4 cells (Fig. 3B). FITC signals from the scrambled aptamer were not detected in all used HER2

negative cell lines. To confirm whether HER2 aptamer can recognize HER2 protiein within non-fixed breast cancer cells cultured in a well, HER2 negative cells were stained with DiI cell tracker and HER2 positive cells unstained (Fig. 3C). The RNA aptamer was clearly detected in HER2 positive cells. The results suggest that HER2 aptamer specifically recognized HER2 expressed cells, which can be useful in a targeting probe for HER2 expressed cancer cells *in vivo*.

Internalization of HER2 targeted aptamer in HER2 positive breast cancer cell lines

Internalization of HER2 aptamer was visualized using confocal microscopy. Breast cancer cell lines were treated with Cy5.5-labeled HER2 aptamer for 30 min at 37 °C and fluorescence signals were observed at 30 min and 6 h after washing out the media (Fig. 4). HER2 aptamer was observed in close association with the cell surface of T47D and KPL4 cells despite cell washing steps. The HER2 aptamer showed minimal uptake in MCF7 and MDA-MB231 cells. After 6 h, internalization of the aptamer was confirmed by visualizing the subcellular distribution of the conjugated Cy5.5 in HER2 positive cells, indicating that HER2 aptamer had accumulated mostly in the perinuclear region, consistent with endosomal routing. In KPL4 cells, Cy5.5-HER2 aptamer showed efficient internalization that was comparable to that observed in T47D cells; in contrast, the fluorescent signal showed minimal uptake in MCF-7 and MDA-MB231 cells lacking HER2 overexpression. This indicates that the internalization of the aptamer was mediated by HER2-dependent targeting.

In vitro uptake of ^{68}Ga-HER2 aptamer

For *in vitro* uptake test with radiolabeled HER2 aptamer, ^{68}Ga was labeled on HER2-specific aptamer. Following purification and washing processes, labeling efficiencies of the ^{68}Ga-aptamer were determined by instant thin layer chromatography (ITLC). ^{68}Ga labeled HER2 aptamer was over 95% (R_f = 0), indicating ^{68}Ga labeled NOTA-HER2 aptamer were successfully labeled and separated. (Fig. 5A). Cell uptake of ^{68}Ga-HER2 aptamer at 37℃ over an incubation period of 1 h is shown in Figure 5B. The probe showed a high and specific uptake in KPL4 cells (24.7 ± 2.5 %CPM/mg). An approximate 2-fold to 2.5-fold increased accumulation of ^{68}Ga-HER2 aptamer in the KPL4 cells was observed compared with other cells, indicating that the probe was specifically targeting HER2.

Animal PET imaging of radiolabeled HER2 aptamer

Tumor images could be generated using radiolabeled HER2 aptamer. Using a PET, coronal images of MDA-MB231 and KPL4 tumor-bearing mice were collected at indicated time points to those for the biodistribution data after tail vein injection of ^{68}Ga-HER2 aptamer (Fig. 6A). ^{68}Ga-HER2 aptamer did not show any tumor uptake in PET imaging. After 28 min, the bladder and liver were predominant, reflecting the 2 major clearance pathways. This means ^{68}Ga-HER2 aptamer was quickly excreted in the urine or hepatic pathway due to short circulation time *in vivo* due to its small size (12,000 Da). For long term monitoring, HER2 aptamer was labeled with ^{64}Cu ($t_{1/2}$ = 12.7 h). PET images were acquired at indicated time pointes

after injection of ^{64}Cu-HER2 aptamer (Fig.6B). However, ^{64}Cu-HER2 aptamer also showed a high renal clearance. Therefore, to use the aptamer as the new imaging probe for PET imaging, new ways to increase the stability and the circulation time of ^{68}Ga-NOTA-aptide *in vivo* needs to be elucidated.

Labeling efficiency and stability of ^{64}Cu-DOTA or -NOTA-HSA

Advantages of albumin as a carrier were biocompatibility and prolonged circulation time *in vivo* (67, 68). In this study, albumins were used as a carrier of targeting ligands, which were labeled with radioisotope such as ^{64}Cu for nuclear imaging. In previous study, differences of ^{64}Cu labeling efficiency and biodistribution patterns were dependent on chelating agent for attaching radioisotope (69). To confirm the radiolabeling efficiency and stability of ^{64}Cu-HSA conjugated NOTA or DOTA, eluted ITLC was counted and measured by the R_f (retention factor) value using TLC scanner. In Figure 7A, ^{64}Cu was labeled on DOTA and NOTA-HSA as well as free SCN-NOTA over time. Following purification and washing processes, ^{64}Cu labeled DOTA-HSA and NOTA-HSA were successfully separated (R_f= 0). To check stability of ^{64}Cu-DOTA and -NOTA-HSA, purified mixtures were incubated in saline and human serum at 37℃ (Fig. 7B). In saline, purified mixtures were stayed at origin on ITLC-SG at initial time. However, at 24 and 48 h, peak of purified mixtures were separated. In case of ^{64}Cu-DOTA-HSA, separated peak was reached up to 1.0 of R_f, and peak of ^{64}Cu-NOTA-HSA was close to 0.5 of R_f at 48 h after incubation. In human serum condition, both ^{64}Cu-DOTA and -NOTA-HSA were separated as soon

as add into the human serum and saline mixture ($R_f \approx 0.7$). At 48 h, percentage of origin peak of ^{64}Cu-DOTA-HSA decreased 51.6% and ^{64}Cu-NOTA-HSA reduced 20.8%. In percentage of movement, ^{64}Cu-DOTA-HSA increased 26.6% and ^{64}Cu-NOTA-HSA was 12.6%. These results demonstrate that ^{64}Cu-NOTA-HSA is more stable than ^{64}Cu-NOTA-HSA in human serum and saline.

In vivo imaging of ^{64}Cu-DOTA or -NOTA-HSA

To compare with *in vivo* stability of ^{64}Cu-DOTA-HSA and ^{64}Cu-NOTA-HSA, human breast cancer cell xenografts in mice were well visualized on the PET images obtained 5 min, 10, 22, 46 h after the intravenous injection of the tracers (Fig. 8). The static PET images of $^{64}CuCl_2$ showed high liver uptake and tumor uptake, presumably from a high level of endogenous CTR1 expression in the liver and tumors (70). In contrast, there was less $^{64}CuCl_2$ uptake in the brain. Diffuse $^{64}CuCl_2$ activity was seen in the abdomen, which represents excretory $^{64}CuCl_2$ activity transported from the liver to the intestinal tract through the bile ducts. Using ^{64}Cu labeled HSA, the static PET images showed high heart and liver uptake. However, there were different distributions of between ^{64}Cu-DOTA-HSA and ^{64}Cu-NOTA-HSA in PET images. In ^{64}Cu-NOTA-HSA, intense tracer activity was present in the heart, liver and brain region, with less tracer activity observed in the abdomen region. Using ^{64}Cu-DOTA-HSA, the probe was observed in the liver and abdomen, but activities of heart and brain regions decreased over time similarly to the PET imaging of $^{64}CuCl_2$. These results suggest that ^{64}Cu-NOTA-HSA is higher stability than ^{64}Cu-DOTA-HSA. In

addition, the difference in stability of ^{64}Cu-NOTA and ^{64}Cu-DOTA complexes certainly played a role.

Analysis of HSA-aptamer bioconjugates

To confirm the conjugates of HSA and aptamer, the conjugates were analyzed by SDS-PAGE. Conjugates shows a broad band of the NOTA-HSA-HER2 aptamer caused by different numbers of HER2 aptamer molecules linked to HSA (Fig. 9A). The aptamer showed a single band corresponding to an Mw of 12 kDa (Lane 1), while HSA displayed a band corresponding to an Mw of 68 kDa (Lane 2). However, HSA and HER2 aptamer both showed bands corresponding to an Mw of ～250 kDa, which is approximately equal to the total Mw of HSA and aptamer. NOTA-HSA-HER2 aptmaer was then successfully radiolabeled with ^{64}Cu, which confirmed by TLC scan (Fig. 9B). Purification of the radioactive reaction mixtures using a PD-10 column resulted in ^{64}Cu-NOTA-HSA-HER2 aptmaer with a decay-corrected yield of more than more than 60%.

In vitro uptake of ^{64}Cu-HSA-aptamer

To investigate the HER2-binding specificity and affinity of the HSA-HER2 aptamer, cell uptake values were analyzed by *in vitro* binding assay in time- or cell number-dependent conditions and completive binding assay. Cell uptake values of ^{64}Cu-HSA-HER2 aptamer and -scrambled aptamer at 37℃ over incubation periods of 0.5, 1, and 2 h are shown in Figure 10A. ^{64}Cu-HSA-HER2 aptamer slowly

accumulated in the KPL4 cells and reached 4.65 ± 0.46 %CPM/mg of the applied activity per mg of protein concentration at 0.5 h. The uptake of KPL4 cells increased to 8.0 ± 0.36 %CPM/mg at 2 h, but not in MDA-MB468 cells (4.65 ± 0.54 %CPM/mg at 2 h). An increase uptake pattern of KPL4 cells was also observed for ^{64}Cu-HSA-HER2 aptamer in a cell number-dependent manner (Fig. 10B). In KPL4 cells, the uptake increased from 4.06 ± 0.99% in 0.156 x 10^6 cells up to 27.71 ± 0.91% in 10 x 10^6 cells. Uptake pattern of ^{64}Cu-HSA-SC was a slight increase up to 11.38 ± 1.01% in 10 x 10^6 cells. However, MDA-MB468 cells showed significantly lower uptakes of both probes at all incubations (around 7% in 10 x 10^6 cells). To further compare with binding affinity of HSA-aptamer, NOTA-aptamer and aptamer-biotin, competitive binding assay was performed with ^{64}Cu-HER2 aptamer and non-radiolabeled probes as competitors. In KPL4 cells, uptake of ^{64}Cu-HER2 aptamer was significant decrease in a dose-dependent manner. The 50% inhibitory concentration (IC50) values for the HSA-aptamer, NOTA-aptamer and aptamer-biotin were estimated to be 1.44 ± 0.23 nM, 12.97 ± 0.23 and 9.68 ± 0.26 nM respectively, whereas no inhibitory activity was observed for the negative controls and MDA-MB468 cells.

These results clearly demonstrate not only specific HER2 receptor binding abilities of both ^{64}Cu-HSA-HER2 aptamer and HER2 aptamer but also increasing uptake values of HSA conjugated aptamer.

Small animal PET imaging of tumor-bearing mice

Decay-corrected coronal PET images of a mouse bearing KPL4 and MDA-MB468 tumors at 5 min, 10, 22, and 46 h after tail vein injection of ^{64}Cu-HSA-HER2 aptamer, -scrambled aptamer and ^{64}Cu-HSA are shown in Figure 11A. For ^{64}Cu-HSA-HER2 aptamer, the KPL4 tumor was visible with a low tumor-to-background contrast at 5 min p.i., but with a good tumor-to-background contrast at 10 and 22 h p.i. The tumor was still clearly detected at 46 h p.i. Quantification analysis revealed that the KPL4 tumor uptake values increased with time and were found to be 1.67 ± 0.39, 4.68 ± 1.13, 5.72 ± 1.34, and 6.63 ± 0.88 %ID/g at 5 min, 10, 22, and 46 h, respectively (Fig. 11B). This activity was about 2.5-fold higher than that measured from the MDA-MB468 tumor region (2.0 ± 0.5 %ID/g at 22 h). As expected, a high tracer uptake (17.5 ± 3.9 %ID/g at 22 h) was determined in the liver. The *in vivo* tumor-targeting specificity was further proven by coinjection of the nonradioactive ^{64}Cu-HSA-HER2 aptamer (Fig. 11C). Compared to nontreated groups, coinjection of large excess of HSA-HER2 aptamer could significantly reduce the KPL4 tumor uptake to around 43.6% of the corresponding uptake at 22 h p.i. (4.73 %ID/g vs 2.66 %ID/g).

Biodistribution of HER2 specific ^{64}Cu-aptamer and ^{64}Cu-HSA-aptamer

The *in vivo* biodistribution of ^{64}Cu-HER2 aptamer and ^{64}Cu-HSA-HER2 aptamer was examined in KPL4 and MDA-MB468 human breast tumor-bearing mouse model. The biodistribution of the ^{64}Cu-HER2 aptamer at 1 and 22 h are shown

in Figure 12A. Slow and high levels of radioactivity accumulation in the KPL4 tumors were observed. The tumor uptake in KPL4 tumors measured was 1.72 %ID/g at 1 h and continually increased to 2.63 %ID/g at 22 h. The ^{64}Cu-HER2 aptamer also displayed relatively slow blood clearance. Blood values of 2.20 %ID/g and 1.34 %ID/g were observed at 1 and 22 h after injection, respectively. Furthermore, ^{64}Cu-HER2 aptamer displayed high levels of liver uptake at indicated time points (20.19 %ID/g and 7.47 %ID/g at 1 and 22 h after injection). The biodistribution of the ^{64}Cu-HSA-HER2 aptamer at 1 and 22 h are shown in Figure 12B. Comparing the biodistribution of ^{64}Cu-HER2 aptamer and ^{64}Cu-HSA-HER2 aptamer at 22 h p.i., the tumor uptake in KPL4 tumors measured was 4.74 %ID/g at 1 h and continually increased to 8.98% ID/g at 22 h, which was significantly higher than that of ^{64}Cu-HER2 aptamer. The ^{64}Cu-HSA-HER2 aptamer also displayed relatively slow blood clearance. Blood values of 5.24 and 3.64 %ID/g were observed at 1 and 22 h after injection, respectively. Furthermore, ^{64}Cu-HSA-HER2 aptamer displayed high levels of liver uptake at all-time points (27.91 and 15.37 %ID/g at 1 and 22 h after injection). The kidneys, however, showed a moderate radioactivity accumulation (9.17 and 9.00 %ID/g at 1 and 22 h after injection, respectively). These data suggest that the probes were cleared predominantly through the hepatobiliary system and to a minor part through the renal system. The *in vivo* tumor-targeting specificity was further proven by coinjection of the nonradioactive ^{64}Cu-HSA-HER2 aptamer. Compared to nontreated groups, coinjection of large excess of HSA-HER2 aptamer could significantly reduce the KPL4 tumor uptake to around 52.6% of the corresponding

uptake at 22 h p.i. (8.98 %ID/g vs 4.73 %ID/g). Consequently, the tumor-to-muscle ratio was significantly decreased for the blocking group (9.19 vs 5.51). Interestingly, the uptake of ^{64}Cu-HER2 aptamer dropped significantly in all major organs from 1 h p.i. to 22 h p.i., while the uptake of ^{64}Cu-HSA-HER2 aptamer remained stable in all organs. This phenomenon may be attributed to the longer circulation half-life of ^{64}Cu-HSA-HER2 aptamer, which resulted in sufficient amount of the tracer circulating in the blood available for antigen binding, whereas ^{64}Cu-HER2 aptamer was gradually cleared with little extra tracer available within the circulation. Comparing 1 and 22 h after injection of ^{64}Cu-HSA-HER2 aptamer, increased uptake of KPL4 tumor was higher than all major organs in the mice, thus providing good tumor contrast (Fig. 12B). Overall, the quantification results obtained from biodistribution studies and PET scans matched very well, confirming that quantitative ROI analysis of noninvasive microPET scans accurately reflected the distribution of PET tracers *in vivo*.

Accumulation of HSA-aptamer in tumor tissues

To investigate whether HSA-aptamer and aptamer were also detected in tumor tissues, KPL4 and MDA-MB468 cells were injected into flanks of BALB/c nude mice. Twenty-two hours after injection of the tracers, tumor tissues were isolated and then sliced for autoradiogram (Fig. 13A). Radioactivity of ^{64}Cu-HSA-HER2 aptamer in HER2-positive KPL4 cells was stronger than that in HER2-negative MDA-MB468 cells. If the ^{64}Cu-HSA aptamer and ^{64}Cu-HER2 aptamer were to specifically bind to HER2 *in vivo*, the distributed pattern of radioactivity would match the pattern of HER2 expression. The localizations of FITC signal in KPL4 tumor

indeed correspond to the distribution of the HER2 positive cells, which are recognized to HER2 protein in tumor tissue (Fig. 13B). These results demonstrated that HSA conjugated HER2 aptamer was more efficient to target HER2 protein than that of HER2 aptamer.

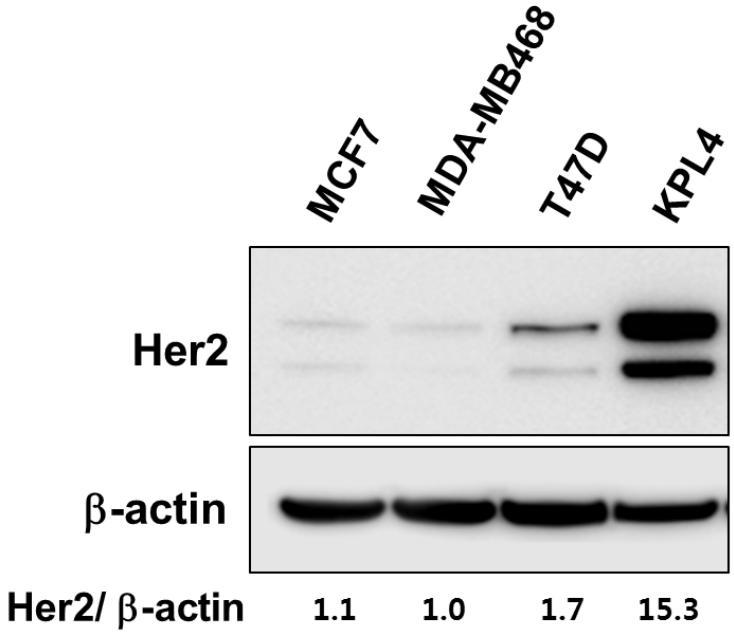

Figure 1. HER2 protein levels in breast cancer cell lines

Total proteins from breast cancer cell lines (MCF7, MDA-MB468, T47D and KPL4) were isolated using RIPA buffer. Total cell lysates were subjected to SDS-PAGE followed by western blot using anti-HER2 specific antibodies. The relative amount of proteins on the blots was determined by Multi Gauge software. Western blot analysis confirmed high-level expression of HER2 in KPL4 cells and weak expression in T47D cells compared with MDA-MB468 and MCF7. β-actin was used as a loading control.

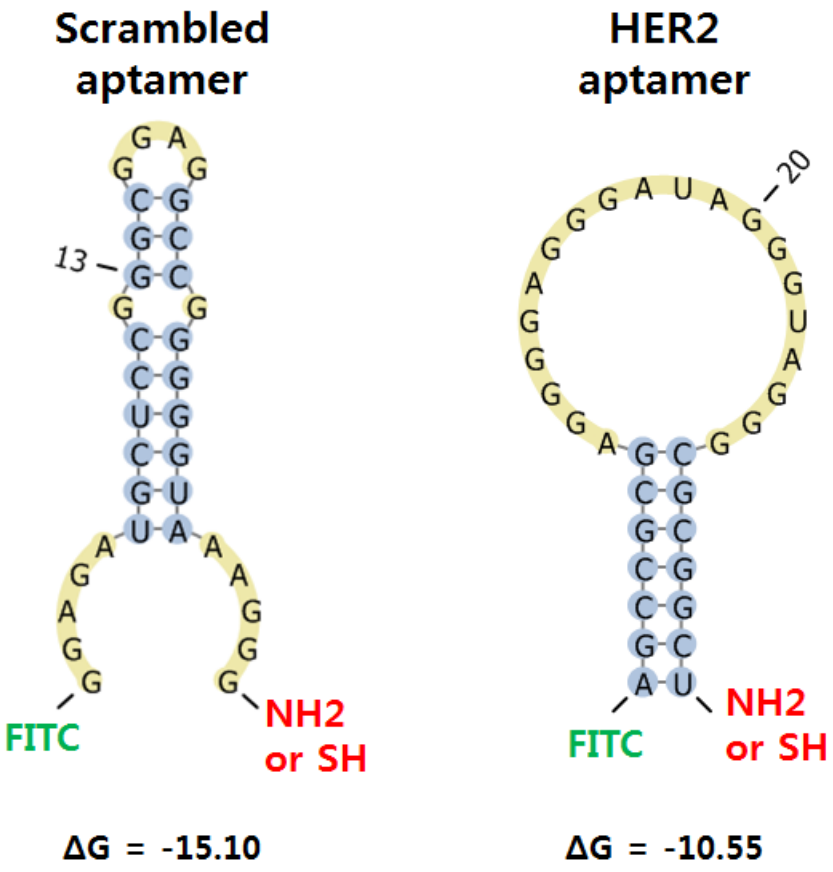

Figure 2. Schematic secondary structure of RNA aptamers

Predicted structure of RNA aptamers (34 mer) for HER2 targeting or scrambled as a control aptamer. Cytocine and uracil of RNA aptamers were modified by replacing the 2′ position with a fluoro (F) group for enhanced nuclease resistance. For *in vitro* and *in vivo* imaging, FITC was conjugated on 5′ region of aptamers and 3′ regions were conjugated with amine (NH_2) or thiol (SH) group.

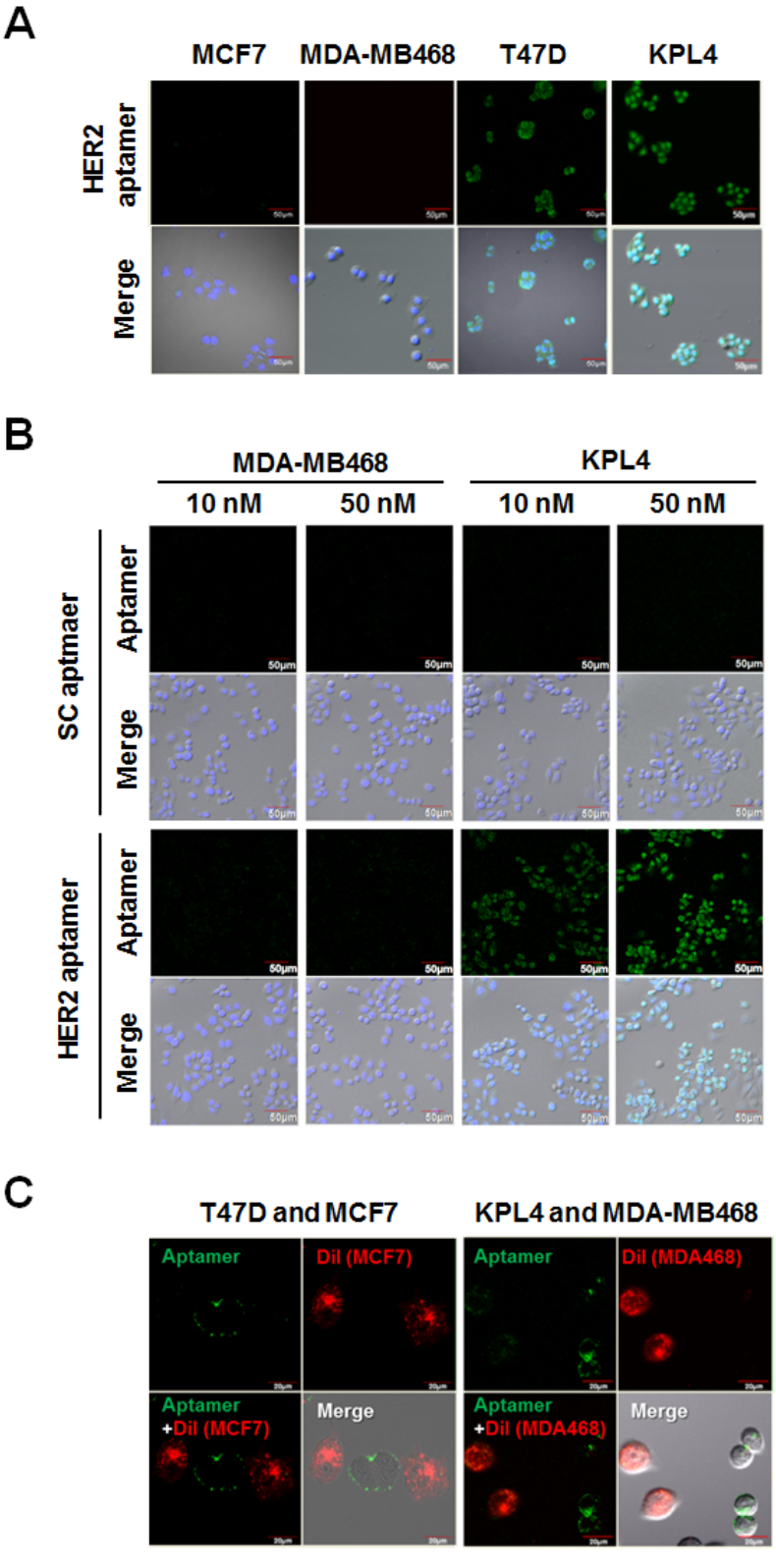
A
MCF7
MDA-MB468
T47D
KPL4
HER2 aptamer
Merge
B
MDA-MB468
KPL4
10 nM
50 nM
10 nM
50 nM
SC aptmaer
Aptamer
Merge
HER2 aptamer
Aptamer
Merge
C
T47D and MCF7
KPL4 and MDA-MB468
Aptamer
Dil (MCF7)
Aptamer
Dil (MDA468)
Aptamer
+Dil (MCF7)
Merge
Aptamer
+Dil (MDA468)
Merge

Figure 3. Specific recognition of HER2-expressing cancer cells by FITC-HER2 aptamer

(A, B) Cells were incubated with FITC-HER2 aptamer (10 or 50 nM) for 1 h. Targeted imaging was obtained by confocal microscopy in fixed cells. (C) HER2 negative cells were pre-incubated with DiI cell tracker. DiI labeled cells (MCF7, MDA-MB468) and non-labeled HER2 positive cells (T47D, KPL4) were incubated in same well of an 8-well chamber slide, respectively. HER2 targeting aptamer (100 nM) treated to the co-culture of cells for 30 min followed by detection of fluorescence signal in non-fixed condition using confocal microscopy. HER2 aptamer specifically recognized HER2 expressed cells.

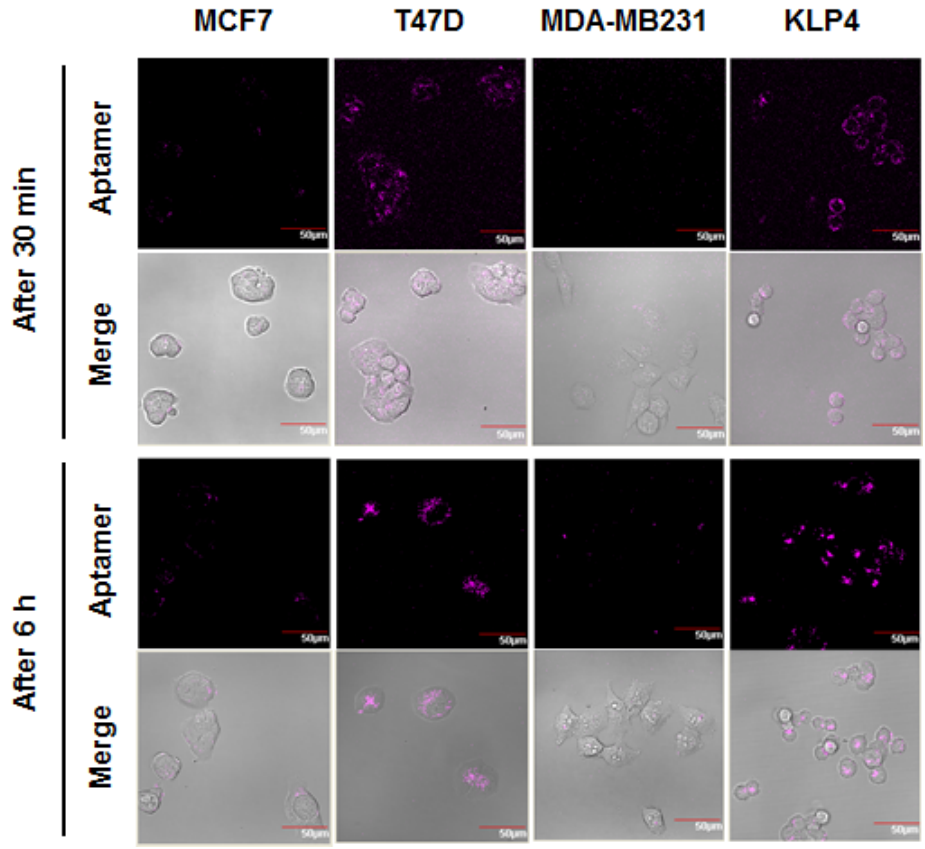

Figure 4. Internalization of targeted aptamer in HER2 positive breast cancer cell lines

Breast cancer cell lines (MCF7, T47D, MDA-MB231 and KPL4) were treated with the HER2 aptamer (100 nM) for 30 min in 8-well chamber slide. The cells were washed and changed fresh culture media. The fluorescent signals were obtained from the cells at 30 min and 6 h after treatment in same cells respectively. Internalization of the aptamer was observed in HER2 positive breast cancer cell lines, KPL4 and T47D.

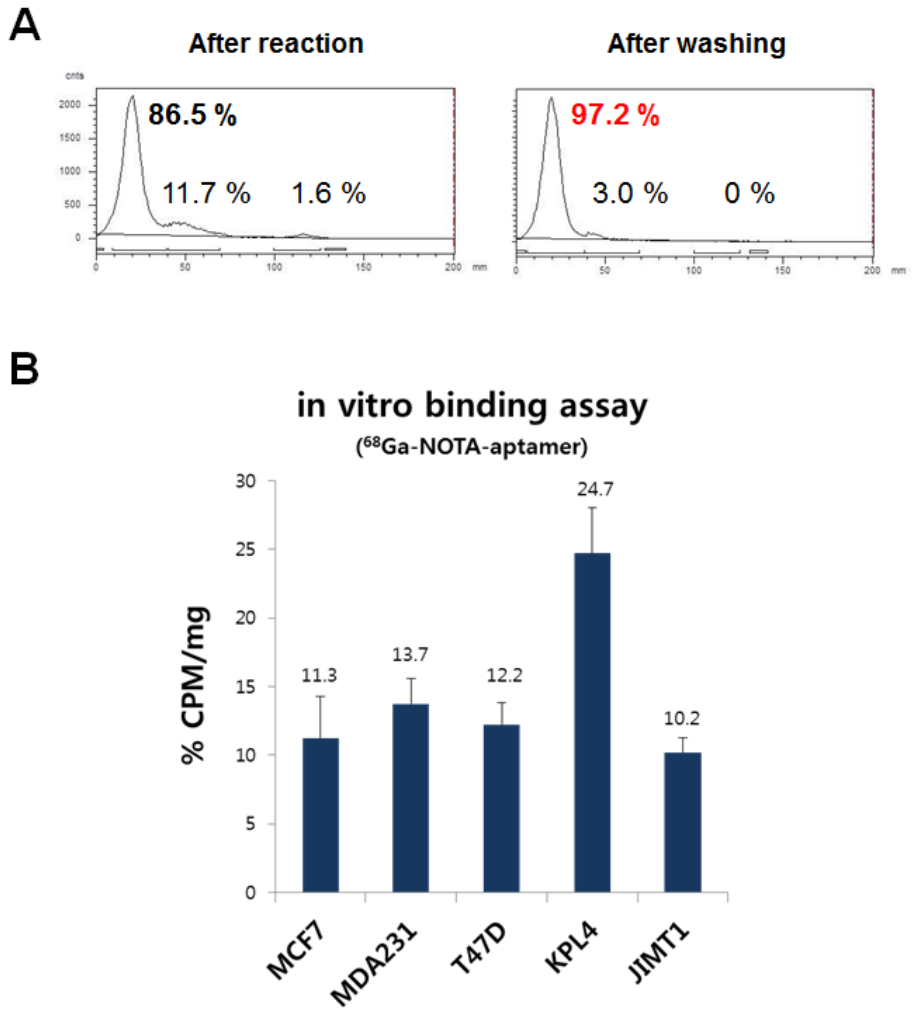

Figure 5. *In vitro* uptake of ^{68}Ga-HER2 aptamer

(A) ITLC chromatograms of ^{68}Ga-HER2 aptamer. ^{68}Ga-HER2 aptamer was labeled at 95℃ for 30 min in heating block. The labeling efficiency of ^{68}Ga-HER2 aptamer was determined using ITLC-SG in 0.1 M citric acid. (B) *In vitro* uptake test using ^{68}Ga-HER2 aptamer in breast cancer cell lines. Cells were plated in 24-well culture plate, and incubated with ^{68}Ga-HER2 aptamer for 1 h. Uptake of ^{68}Ga-HER2 aptamer was counted by γ-counter. And measured radioactivity was normalized by protein concentration from cell lysates. In the KPL4 cells, an around 2-fold increased accumulation of ^{68}Ga-HER2 aptamer was observed compared with other cells.

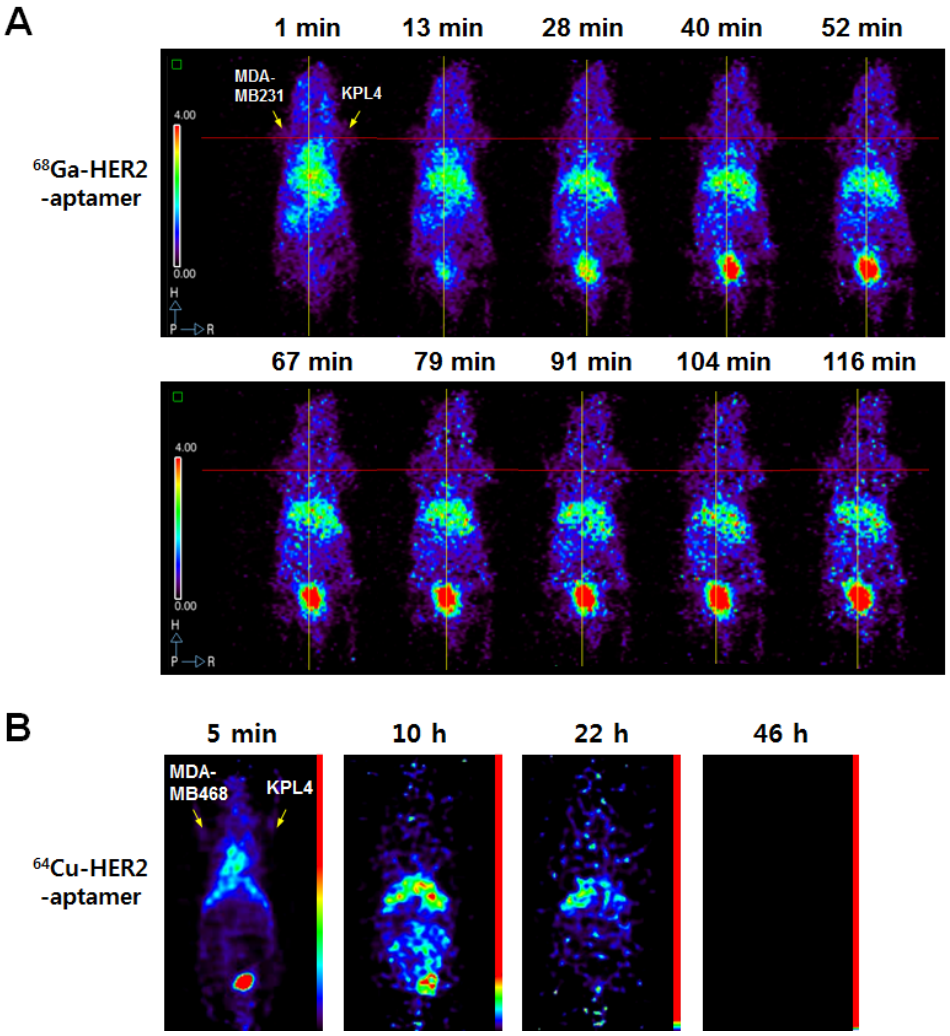

Figure 6. PET imaging of radiolabeled HER2 aptamer in xenograft models

(A) PET images of ^{68}Ga-HER2 aptamer were acquired in KPL4 and MDA-MB231 tumors at indicated time points after tail vein injection of ^{68}Ga-HER2 aptamer. Arrows indicate the location of tumors. (B) Serial PET images of ^{64}Cu-HER2 aptamer were acquired in nude mice bearing KPL4 and MDA-MB468 tumors. Representative coronal PET images at 5 min, 10, 22, and 46 h after tail vein injection of ^{64}Cu-HER2 aptamer. Arrows indicate the location of tumors. Radiolabeled HER2 aptamer did not how any tumor uptake in serial PET images.

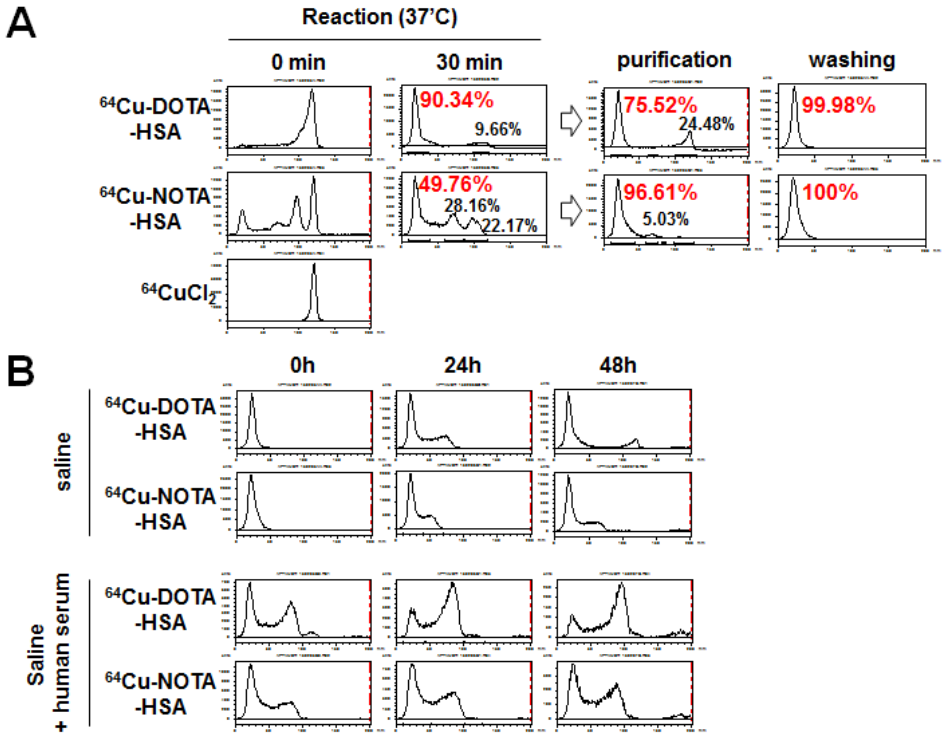

Figure 7. Labeling efficiency and stability of ^{64}Cu-DOTA- or -NOTA-HSA

(A) ^{64}Cu-DOTA or -NOTA-HSA were labeled at 37℃ for 1 h in heating block. The labeling efficiency of ^{64}Cu-DOTA- or - NOTA-HSA was detected in ITLC-SG, eluted with 0.1 M sodium citrate. (B) Stability test of ^{64}Cu-DOTA- or - NOTA-HSA in saline and human serum at 37℃. The stability of ^{64}Cu-DOTA- or - NOTA-HSA was detected in ITLC-SG, eluted with 0.1 M sodium citrate.

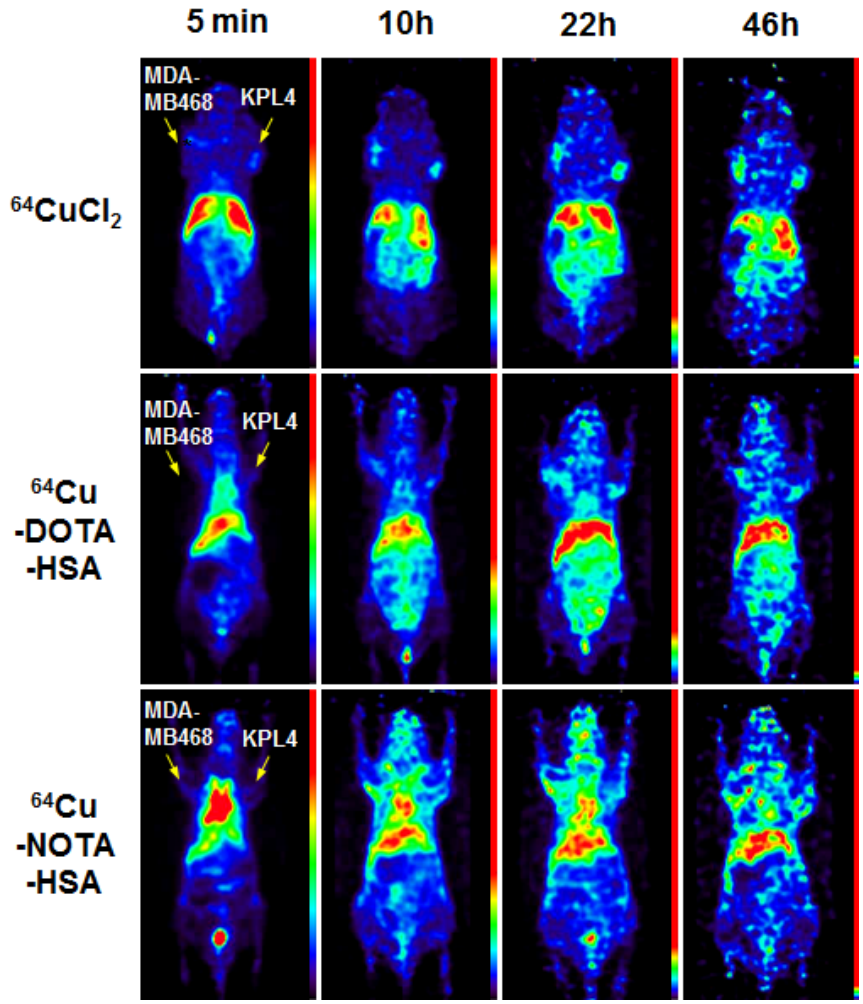

Figure 8. ***In vivo*** **PET imaging of ^{64}Cu-DOTA- or -NOTA-HSA**

Serial PET images were acquired in nude mice bearing KPL4 and MDA-MB468 tumors. Representative coronal PET images at 5 min, 10, 22, and 46 h after tail vein injection of $^{64}CuCl_2$, ^{64}Cu-DOTA-HSA and ^{64}Cu-NOTA-HSA, respectively. Arrows indicate the location of tumors. In ^{64}Cu-NOTA-HSA, intense tracer activity was present in the heart, liver and brain region, with less activity observed in the abdomen regions. Using ^{64}Cu-DOTA-HSA, activities of heart and brain regions decreased over time similarly to the PET imaging of $^{64}CuCl_2$.

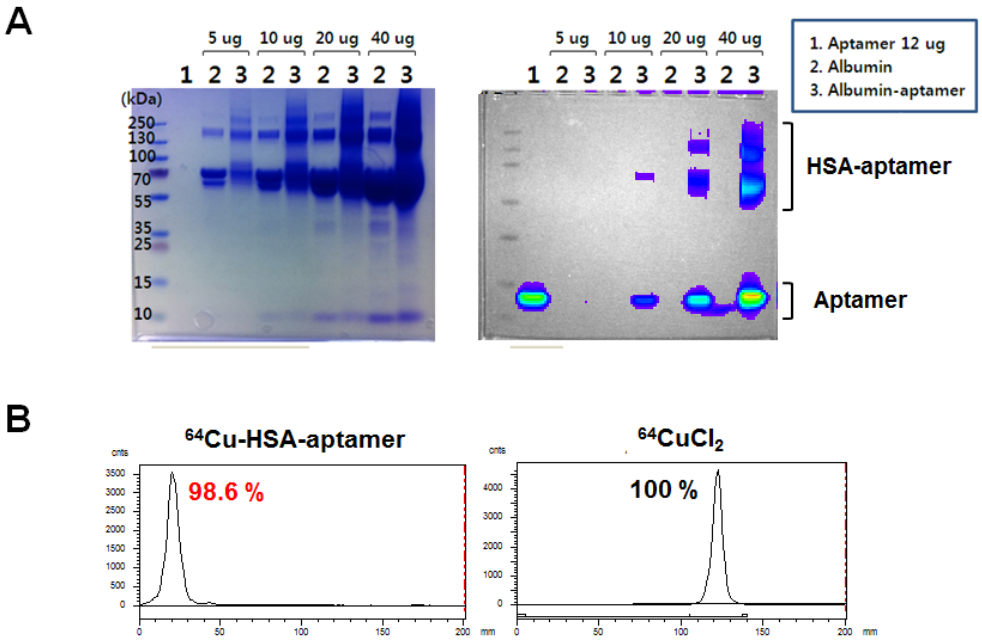

Figure 9. Aptamer-HSA bioconjugates

(A) SDS-PAGE analysis of reaction mixtures obtained from the chemical conjugation procedure of HSA with HER2 aptamer. Conjugation of HSA and aptamer was confirmed by coomassie blue staining and IVIS imaging system. 1, aptamer-FITC; 2, HSA; 3, HSA-HER2 aptamer-FITC (B) NOTA-HSA-HER2 aptamer were labeled with $^{64}CuCl_2$ at 37℃ for 1 h in heating block. The labeling efficiency of ^{64}Cu-HSA-HER2 aptamer was detected in ITLC-SG, eluted with 0.1 M sodium citrate. NOTA-HSA-HER2 aptmaer was successfully radiolabeled with ^{64}Cu.

A

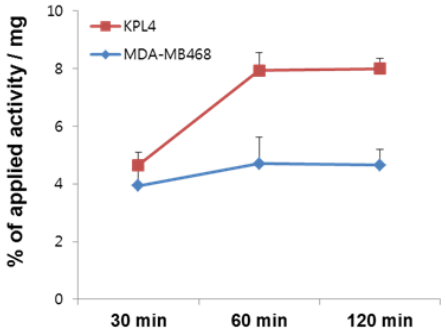
KPL4
MDA-MB468
% of applied activity / mg
10
8
6
4
2
0
30 min
60 min
120 min

B

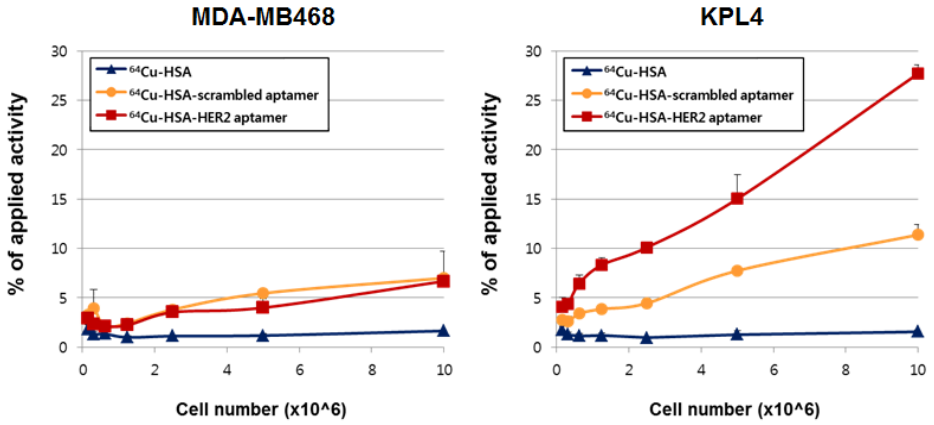
MDA-MB468
KPL4
64Cu-HSA
64Cu-HSA-scrambled aptamer
64Cu-HSA-HER2 aptamer
% of applied activity
Cell number (x10^6)

C

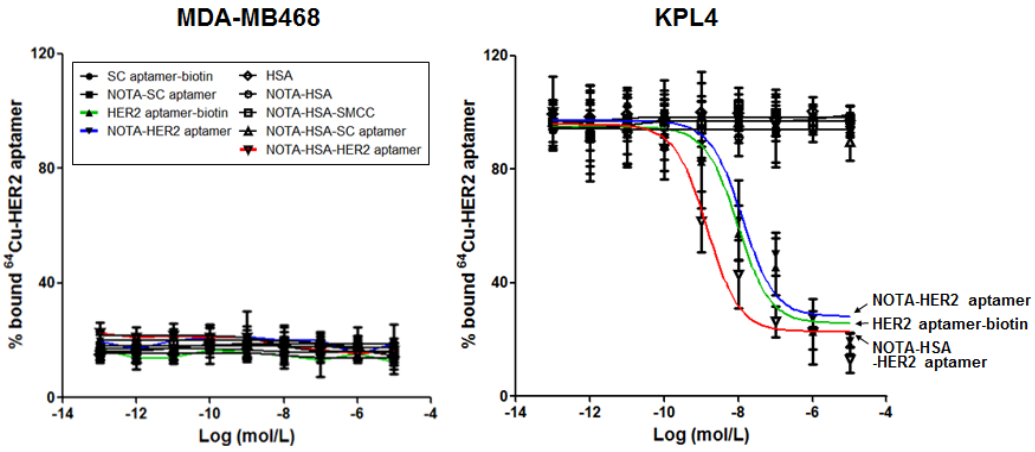
MDA-MB468
KPL4
SC aptamer-biotin
NOTA-SC aptamer
HER2 aptamer-biotin
NOTA-HER2 aptamer
HSA
NOTA-HSA
NOTA-HSA-SMCC
NOTA-HSA-SC aptamer
NOTA-HSA-HER2 aptamer
% bound 64Cu-HER2 aptamer
Log (mol/L)
NOTA-HER2 aptamer
HER2 aptamer-biotin
NOTA-HSA
-HER2 aptamer

Figure 10. *In vitro* uptake test of ^{64}Cu-HSA-aptamer

(A) Uptake of ^{64}Cu-HSA-HER2 aptamer in KPL4 and MDA-MB468 cells over time at 37℃. (B) Uptake of ^{64}Cu-HSA-HER2 aptamer, -scrambled aptamer and ^{64}Cu-HSA in serial diluted KPL4 and MDA-MB468 cells for 1 h after the treatment at 37℃. (C) *In vitro* competitive binding assay, inhibition of ^{64}Cu-HER2 aptamer binding to HER2 on KPL4 and MDA-MB468 cells by aptamers, HSA and HSA-aptamers. All results are expressed as a percentage of applied radioactivity and are means of three measurements ± SD. Both ^{64}Cu-HSA-HER2 aptamer and HER2 aptamer bound to HER2 positive breast cancer cells and HSA-HER2 aptamer increased uptake values compared to only HER2 aptamer. The IC50 values for the HSA-aptamer, NOTA-aptamer and aptamer-biotin were estimated to be 1.44 ± 0.23 nM, 12.97 ± 0.23 and 9.68 ± 0.26 nM, respectively.

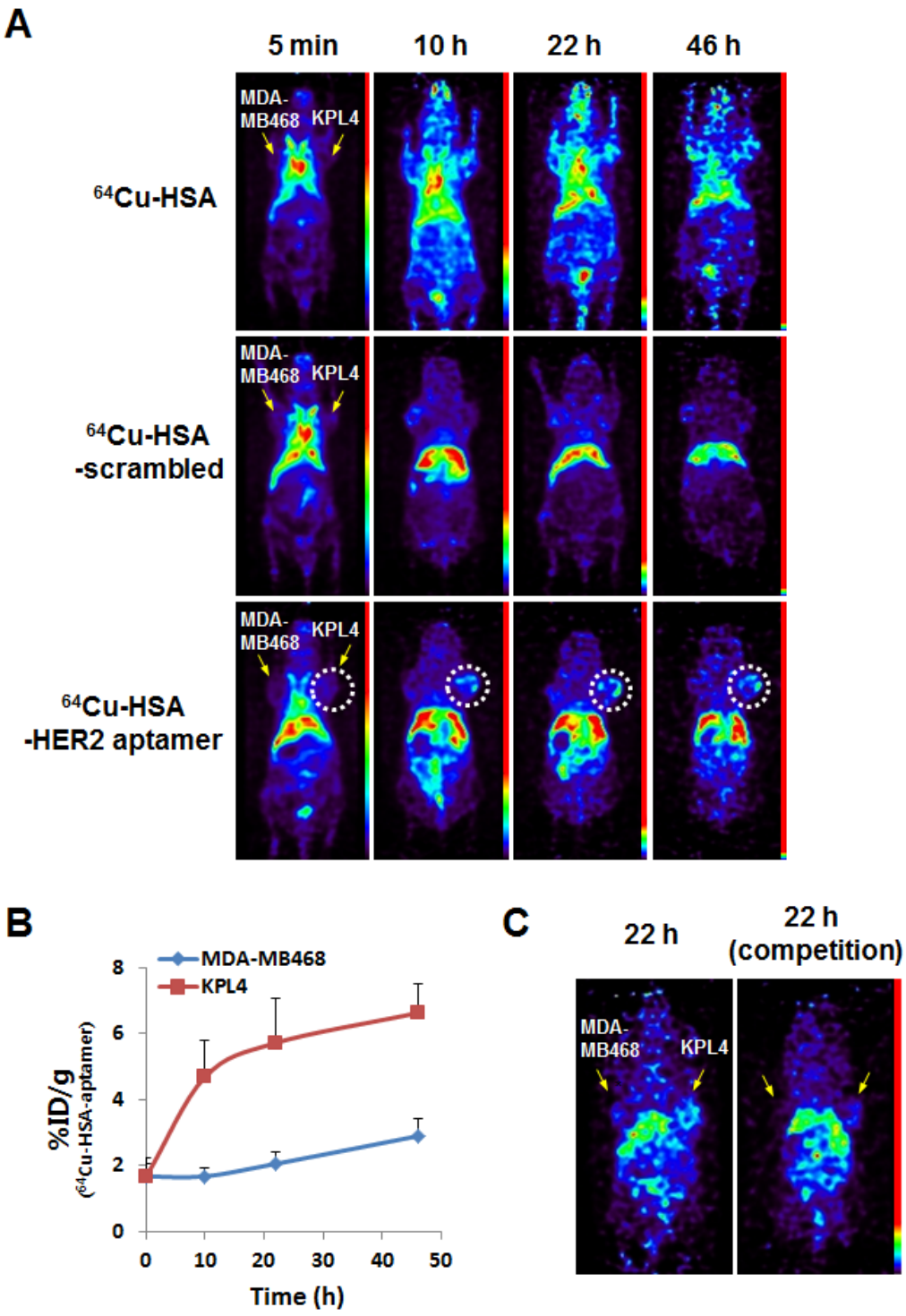
A
5 min
10 h
22 h
46 h
MDA-MB468
KPL4
64Cu-HSA
64Cu-HSA -scrambled
64Cu-HSA -HER2 aptamer
B
MDA-MB468
KPL4
%ID/g (64Cu-HSA-aptamer)
Time (h)
C
22 h
22 h (competition)

Figure 11. ***In vivo*** **tumor imaging of ^{64}Cu-HSA-aptamer**

(A) Micro-PET imaging in nude mice bearing KPL4 and MDA-MB468 tumors. Representative decay-corrected coronal PET images at 5 min, 10, 22, and 46 h after tail vein injection of ^{64}Cu-HSA-HER2 aptamer, -scrambled aptamer and ^{64}Cu-HSA as control. (B) Tumor time-activity curves derived from multiple-time-point small-animal PET images after tail vein injection of ^{64}Cu-HSA-HER2 aptamer. Data presented are shown as mean ± SD %ID/g (n = 3). (C) PET imaging of ^{64}Cu-HSA-HER2 aptamer in KPL4 and MDA-MB468 tumors in the presence or absence of nonradioactive HSA-HER2 aptamer. Arrows indicate the location of tumors. The KPL4 tumor uptake of ^{64}Cu-HSA-HER2 aptamer was about 2.5-fold higher than that measured from the MDA-MB468 tumor region.

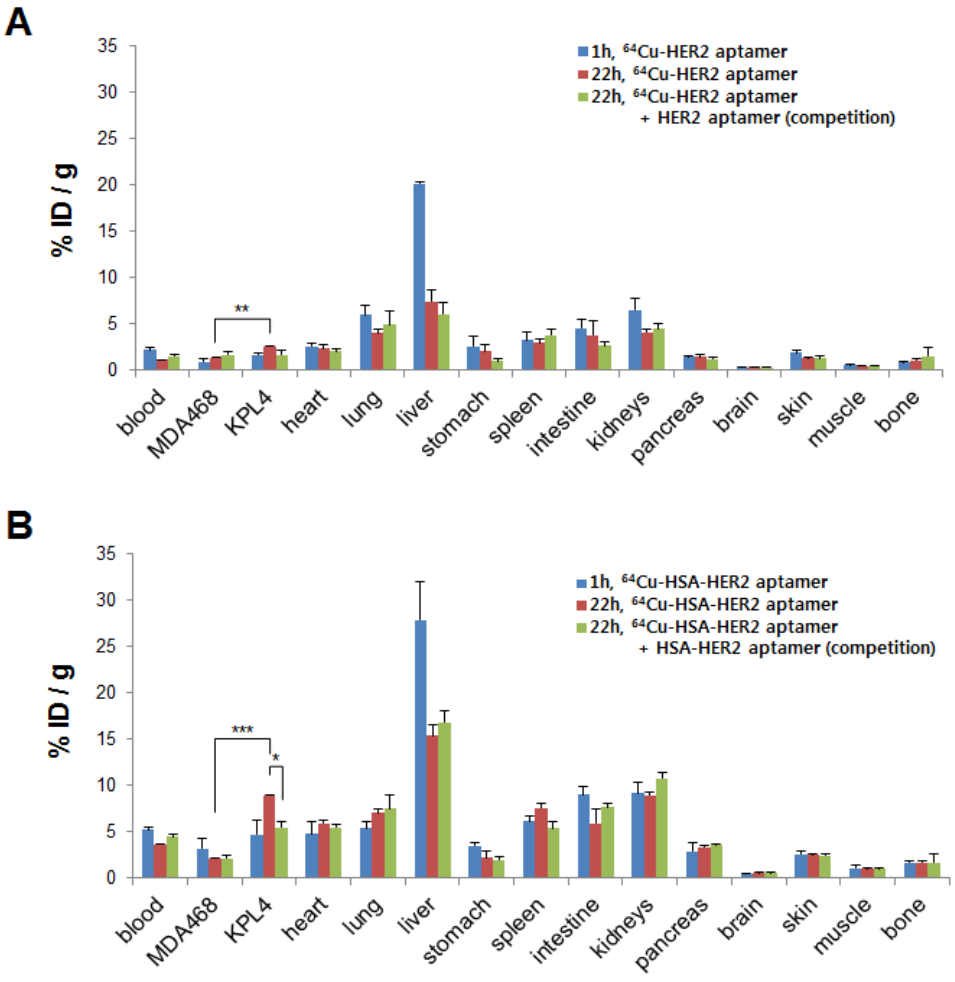

Figure 12. Biodistribution of ^{64}Cu-HER2 aptamer and ^{64}Cu-HSA-HER2 aptamer

In KPL4 and MDA-MB468 tumor-bearing mice, data are expressed as the percentage administered activity (injected dose) per gram of tissue (%ID/g) after intravenous injection of (A) ^{64}Cu-HER2 aptamer and (B) ^{64}Cu-HSA-HER2 aptamer at 1 and 22 h (n = 3), respectively. For 22 h-block, mice were coinjected with the radioactive and nonradioactive HSA-HER2 aptamer (n = 3). Comparing the biodistribution of ^{64}Cu-HER2 aptamer and ^{64}Cu-HSA-HER2 aptamer, the tumor uptake in KPL4 tumors was significantly higher than that of ^{64}Cu-HER2 aptamer. (*, $P < 0.01$; **, $P < 0.005$; ***, $P < 0.001$; two-tailed t-test)

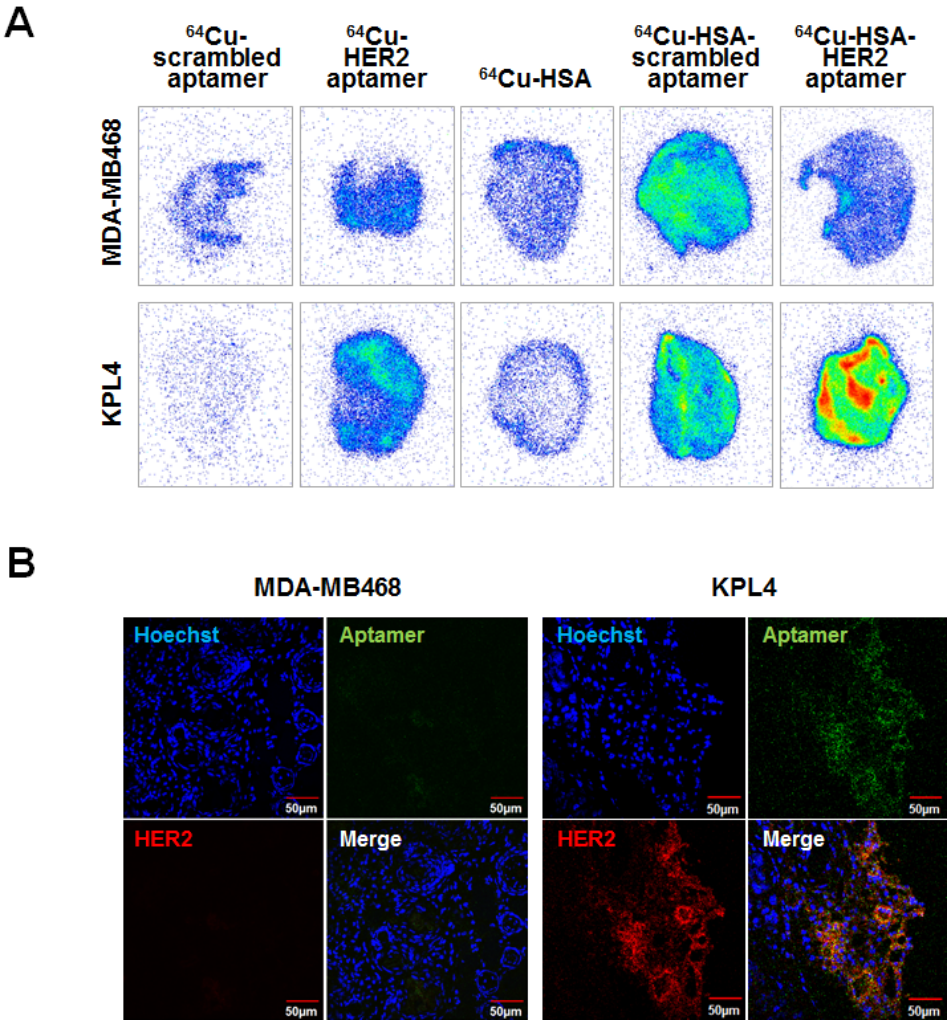

Figure 13. Accumulation of ^{64}Cu-HER2 aptamer and ^{64}Cu-HSA-HER2 aptamer in tumor tissues

(A) Autoradiogram in tissue sections of KPL4 and MDA-MB468 tumor-bearing mice at 22 h after tail vein injection of indicated probes. (B) Immunofluorescence localization of HER2 used a rabbit antibody, as well as a secondary, fluorescent labeled antibody in tumor tissues. DAPI was used to visualize nuclei. HSA conjugated HER2 aptamer was more efficient to target HER2 expressing cells than that of HER2 aptamer.

Discussion

HER2 overexpression is found not only in 20-30% of breast cancers, but also in gastric, ovarian, bladder, and lung cancers (71-77). Therefore, HER2 may serve as a potential target for targeted tumor therapy against many malignancies. Monoclonal antibodies have been the main approach for HER2-targeted cancer imaging and therapy, and trastuzumab (Herceptin), a humanized HER2 monoclonal antibody, has been approved as a treatment for HER2-positive breast cancer. However, drug resistance is commonly and rapidly developed with trastuzumab treatment (6, 7, 20-23), making it necessary to explore other HER2-targeting therapeutic strategies. Recent studies have identified some RNA or DNA HER2 aptamers (39, 41), which are single-stranded oligonucleotides that bind to their target with high affinity and specificity, and may serve as targeting molecules in therapeutic and diagnostic applications (28). Kim developed an RNA aptamer using HER2 protein as the target, and proposed that the selected aptamer could potentially be utilized in constructing novel imaging agents for HER2-positive cancers. Binding affinity of developed HER2 aptamer was about $3.49 \pm 1.3 \times 10^{-9}$ M (41). Despite these advantages, the use of aptamer molecules for radiotherapeutic applications is questionable, mainly due to their relatively fast renal clearance (compared to antibody) (78-81). In this study, both ^{68}Ga-labeled and ^{64}Cu- labeled HER2 aptamer also had fast renal clearance. Based on previous reports and results, in order to improve the blood circulation and targeting efficiency *in vivo*, HER2 aptamer was conjugated with HSA that has a long

circulating half-life and is not eliminated through the kidneys. The conjugates were radiolabeled with the PET radionuclide ^{64}Cu, which were evaluated for the efficiency of tumor targeting and the biodistribution.

In vivo stability of ^{64}Cu-chelates is important to PET imaging, which has been hotly debated over the last decade, and many chelators have been designed and evaluated for ^{64}Cu-labeling of various targeting agents (50). Based on available literature data, the *in vitro* thermodynamic stability constants of Cu-DOTA and Cu-NOTA are similar at 25℃ (82, 83). However, these constants were measured in a simple *in vitro* chemical system, which does not represent the biological environment *in vivo*. Furthermore, attaching a probe to the chelator will significantly improve the stability of the ^{64}Cu-chelator complex, since trans-chelation of Cu requires conformational change of the chelator, which is much more difficult when a probe is attached. In this study, the *in vivo* behavior of DOTA-HSA and NOTA-HSA was monitored by PET imaging. The two conjugates showed similar distributed imaging at 5 min p.i. However, tracer uptake in many organs exhibited significant differences, including the heart, liver, intestine, and brain. Liver and intestine uptake of ^{64}Cu-DOTA-HSA was much higher than that of ^{64}Cu-NOTA-HSA at 10, 22, 46 h p.i. Heart uptake of ^{64}Cu-NOTA-HSA was also much higher than that of ^{64}Cu-DOTA-HSA at all indicated times p.i.(Figure 8), which is likely due to the more stable complex and prolonged circulation half-life of ^{64}Cu-NOTA-HSA. Since the majority of ^{64}Cu is absorbed by the liver and excreted into the intestinal tract through bile ducts via copper transport receptors (CTR) (70, 84), uptake of ^{64}Cu-DOTA-HSA in liver and

intestine represented that ^{64}Cu was released from the conjugates. One possible explanation for this finding is the increased number of carboxyl (-COOH) groups of SCN-DOTA compared with SCN-NOTA. It was considered that either an extra carboxyl group encounters phagocytic cells in liver or Cu is loosely fitted into DOTA structure, resulting in the dissociation of Cu from DOTA.

For HER2 targeted PET imaging, the synthesis of chemically conjugated NOTA-HSA-aptamer was performed in three steps. First, HSA was modified with the metal chelator NOTA. It was found that two NOTA were coupled with one HSA molecule (85). The conjugation of NOTA to the backbone of HSA as the first step is advantageous and avoids a potential unfavorable modification of the aptamer. Second, the bifunctional cross-linker sulfo-SMCC was conjugated to NOTA-HSA through lysine residues. In the third step, the HER2 aptamer was covalently conjugated with NOTA-HSA-SMCC. It was found that aptamer molecules were covalently conjugated onto HSA molecule. The chemical conjugation of aptamer molecules to HSA has several distinctive advantages compared to monoclonal antibody or fusion proteins. First, the method avoids time-consuming techniques, such as molecular cloning and protein purification. Moreover, compared to monoclonal antibody, the conjugation used in this study could allow for a quick and efficient conjugation of many other targeting ligands in a similar fashion. Second, the HSA modification not only improves the prolonged blood circulation of the aptamer due to a higher molecular weight, but ligand conjugated HSA also increases the chance of binding to the target molecules. This may allow multiple and simultaneous binding to HER2 receptors and

lead to an improved tumor targeting efficacy and retention. Third, HSA is less susceptible to stability problems in clinical usage in comparison with other metal-based nanoparticles. HSA, the most prominent protein in plasma, is one of the most extensively investigated proteins. HSA is synthesized in the liver and exported as a single non-glycosylated chain, reaching a blood concentration of about 7.0×10^{-4} M (67). The half-life of HSA is approximately 15-20 days. And HSA is biocompatible and has a prolonged circulation time *in vivo* (67, 68). However, there are several limitations using HSA as a carrier. First, viral or bacterial contamination of manufacturing process can affect product quality. Also, HSA should be stored carefully because the biodegradable material is perishable. Second, the better signal-to-background ratio of the target image is easier to distinguish normal tissues and targets. HSA conjugates could not help improve the signal-to-background ratio due to a long stay in the blood. Images of HSA conjugates could be difficult to distinguish whether the image is targeted signals or blood pool although they accumulate in target regions. Third, HSA itself features high liver uptake. Therefore, HSA conjugated drugs for treatment of tumors may have difficulty in determining therapeutic dose without damage to the normal liver cells.

Another strategy of increasing circulation half-life is the addition of conjugation partners such as polyethylene glycol or cholesterol (86). Conjugation of aptamers to a 40 kDa polyethylene glycol (PEG) polymer (PEGylation) can significantly lengthen residence times of aptamers in circulation while marginally impacting the ability to bind to protein targets (44). Moreover, the capacity of a

cholesterol tag significantly prolonged the plasma half-life of an antisense oligonucleotide (87). However, conjugation with a linear shaped molecules such as PEG and cholesterol can lead to increased blood circulation time of aptamer, but there are limitations to attach only a targeting agent due to small surface area and lack of functional groups. On the other hand, in the case of spherical nanoparticles such as albumin, surface area is larger than those of the linear shaped carriers, which can be useful for conjugation of different or multiple agents.

In this study using HSA as a carrier, NOTA-HSA-aptamer bioconjugates were successfully chemically synthesized and labeled with ^{64}Cu. Evaluation of the radiolabeled conjugates in mice demonstrated that ^{64}Cu-NOTA-HSA-aptamer are promising agents for HER2 imaging. These probes provide high specificity and sensitivity, and display excellent tumor contrasts as shown in PET, biodistribution studies and autoradiogram. For small-animal PET, excellent tumor to background contrast of the KPL4 tumors was obtained at 10, 22, and 46 h after injection of ^{64}Cu-HSA-HER2 aptamer, whereas the MDA-MB468 tumors could be barely seen. And targeted images were not observed in ^{64}Cu-HSA and ^{64}Cu-HSA-scrambled aptamer injected mice as controls (Figure 11). Quantitative analysis of PET images using ^{64}Cu-HSA-HER2 aptamer suggested a significant difference in tumor uptake of ^{64}Cu-HSA-HER2 aptamer. This is a good reflection of the specificity of ^{64}Cu-HSA-HER2 aptamer in HER2-positive tumors. Biodistribution studies revealed a specific binding of ^{64}Cu-HSA-HER2 aptamer to HER2 protein as shown by a reduced KPL4 tumor

uptake after coinjection with HSA-HER2 aptamer (Figure 12). Moreover, HER2 aptamer was improved on circulation half-life by conjugating with HSA.

Further study is required before the efficacy of HSA-aptamer therapy can be examined in preclinical studies. First it is needed to determine the proper dose of ^{64}Cu-HSA-aptamer to maximize the targeting efficiency against cancer cells and to minimize the damage of normal organs. Second, other therapeutic drugs or radionuclides should be conjugated with HSA-aptamer for simultaneous targeted imaging and therapy.

In summary, ^{64}Cu labeled HSA-HER2 aptamer as a molecular imaging probe was developed in this study. The conjugated probe was stable for 46 h in serum and saline condition. *In vivo* PET imaging results proved that the ^{64}Cu-HSA-HER2 aptamer can be targeted to HER2-positive tumor through accumulation in HER2-expressed regions of the tumor tissue at 22 h after injection. This exemplifies their potential for the targeted imaging of HER2-positive cancer. More importantly, the *in vivo* properties and pharmacokinetics of NOTA-HSA-HER2 aptamer conjugates make them promising candidates for labeling with therapeutic radionuclides, such as ^{90}Y or ^{177}Lu. This proof-of-concept research of conjugating HSA to alternate biodistribution of biomolecules such as aptamer indicates a broader application towards many other imaging and radionuclide therapy agents, which will be useful for various diagnostic and therapeutic applications.

REFERENCES

1. Yarden Y, Sliwkowski MX. Untangling the ErbB signalling network. Nature reviews Molecular cell biology. 2001;2(2):127-37.

2. Slamon DJ, Godolphin W, Jones LA, Holt JA, Wong SG, Keith DE, et al. Studies of the HER-2/neu proto-oncogene in human breast and ovarian cancer. Science. 1989;244(4905):707-12.

3. Schneider PM, Hung MC, Chiocca SM, Manning J, Zhao XY, Fang K, et al. Differential expression of the c-erbB-2 gene in human small cell and non-small cell lung cancer. Cancer research. 1989;49(18):4968-71.

4. Yokota J, Yamamoto T, Miyajima N, Toyoshima K, Nomura N, Sakamoto H, et al. Genetic alterations of the c-erbB-2 oncogene occur frequently in tubular adenocarcinoma of the stomach and are often accompanied by amplification of the v-erbA homologue. Oncogene. 1988;2(3):283-7.

5. Slamon DJ, Clark GM, Wong SG, Levin WJ, Ullrich A, McGuire WL. Human breast cancer: correlation of relapse and survival with amplification of the HER-2/neu oncogene. Science. 1987;235(4785):177-82.

6. Garrett JT, Arteaga CL. Resistance to HER2-directed antibodies and tyrosine kinase inhibitors: mechanisms and clinical implications. Cancer biology & therapy. 2011;11(9):793-800.

7. Nahta R, O'Regan RM. Evolving strategies for overcoming resistance to HER2-directed therapy: targeting the PI3K/Akt/mTOR pathway. Clinical breast cancer. 2010;10 Suppl 3:S72-8.

8. Cooke T, Reeves J, Lanigan A, Stanton P. HER2 as a prognostic and predictive marker for breast cancer. Annals of oncology : official journal of the European Society for Medical Oncology / ESMO. 2001;12 Suppl 1:S23-8.

9. Menard S, Fortis S, Castiglioni F, Agresti R, Balsari A. HER2 as a prognostic factor in breast cancer. Oncology. 2001;61 Suppl 2:67-72.

10. Menard S, Casalini P, Campiglio M, Pupa S, Agresti R, Tagliabue E. HER2 overexpression in various tumor types, focussing on its relationship to the development of invasive breast cancer. Annals of oncology : official journal of the European Society for Medical Oncology / ESMO. 2001;12 Suppl 1:S15-9.

11. Li X, Lewis MT, Huang J, Gutierrez C, Osborne CK, Wu MF, et al. Intrinsic resistance of tumorigenic breast cancer cells to chemotherapy. Journal of the National Cancer Institute. 2008;100(9):672-9.

12. King CR, Kraus MH, Aaronson SA. Amplification of a novel v-erbB-related gene in a human mammary carcinoma. Science. 1985;229(4717):974-6.

13. Inwald EC, Ortmann O, Zeman F, Koller M, Hofstadter F, Gerstenhauer M, et al. Guideline Concordant Therapy Prolongs Survival in HER2-Positive Breast Cancer Patients: Results from a Large Population-Based Cohort of a Cancer Registry. BioMed research international. 2014;2014:137304.

14. Ariazi EA, Clark GM, Mertz JE. Estrogen-related receptor alpha and estrogen-related receptor gamma associate with unfavorable and favorable biomarkers, respectively, in human breast cancer. Cancer research. 2002;62(22):6510-8.

15. Wright C, Nicholson S, Angus B, Sainsbury JR, Farndon J, Cairns J, et al. Relationship between c-erbB-2 protein product expression and response to endocrine therapy in advanced

breast cancer. British journal of cancer. 1992;65(1):118-21.

16. Montemurro F, Di Cosimo S, Arpino G. Human epidermal growth factor receptor 2 (HER2)-positive and hormone receptor-positive breast cancer: new insights into molecular interactions and clinical implications. Annals of oncology : official journal of the European Society for Medical Oncology / ESMO. 2013;24(11):2715-24.

17. Press MF, Bernstein L, Thomas PA, Meisner LF, Zhou JY, Ma Y, et al. HER-2/neu gene amplification characterized by fluorescence in situ hybridization: poor prognosis in node-negative breast carcinomas. Journal of clinical oncology : official journal of the American Society of Clinical Oncology. 1997;15(8):2894-904.

18. Valabrega G, Montemurro F, Aglietta M. Trastuzumab: mechanism of action, resistance and future perspectives in HER2-overexpressing breast cancer. Annals of oncology : official journal of the European Society for Medical Oncology / ESMO. 2007;18(6):977-84.

19. Montemurro F, Valabrega G, Aglietta M. Lapatinib: a dual inhibitor of EGFR and HER2 tyrosine kinase activity. Expert opinion on biological therapy. 2007;7(2):257-68.

20. Cobleigh MA, Vogel CL, Tripathy D, Robert NJ, Scholl S, Fehrenbacher L, et al. Multinational study of the efficacy and safety of humanized anti-HER2 monoclonal antibody in women who have HER2-overexpressing metastatic breast cancer that has progressed after chemotherapy for metastatic disease. Journal of clinical oncology : official journal of the American Society of Clinical Oncology. 1999;17(9):2639-48.

21. Vogel CL, Cobleigh MA, Tripathy D, Gutheil JC, Harris LN, Fehrenbacher L, et al. Efficacy and safety of trastuzumab as a single agent in first-line treatment of HER2-overexpressing metastatic breast cancer. Journal of clinical oncology : official journal of the American Society of Clinical Oncology. 2002;20(3):719-26.

22. Raguz S, Yague E. Resistance to chemotherapy: new treatments and novel insights into an old problem. British journal of cancer. 2008;99(3):387-91.

23. Shattuck DL, Miller JK, Carraway KL, 3rd, Sweeney C. Met receptor contributes to trastuzumab resistance of HER2-overexpressing breast cancer cells. Cancer research. 2008;68(5):1471-7.

24. Piccart-Gebhart MJ, Procter M, Leyland-Jones B, Goldhirsch A, Untch M, Smith I, et al. Trastuzumab after adjuvant chemotherapy in HER2-positive breast cancer. The New England journal of medicine. 2005;353(16):1659-72.

25. Modi S, Stopeck AT, Gordon MS, Mendelson D, Solit DB, Bagatell R, et al. Combination of trastuzumab and tanespimycin (17-AAG, KOS-953) is safe and active in trastuzumab-refractory HER-2 overexpressing breast cancer: a phase I dose-escalation study. Journal of clinical oncology : official journal of the American Society of Clinical Oncology. 2007;25(34):5410-7.

26. Burstein H, Awada A, Badwe R, Dirix L, Tan A, Jacod S, et al. HKI-272, an irreversible pan erbB receptor tyrosine kinase inhibitor: preliminary phase 2 results in patients with advanced breast cancer. Breast Cancer Research and Treatment. 2007;106:S268-S.

27. Fumoleau P, Wardley A, Miles D, Verma S, Gelmon K, Cameron D, et al. Safety of pertuzumab plus trastuzumab in a phase II trial of patients with HER2-overexpressing metastatic breast cancer which had progressed during trastuzumab therapy. Breast Cancer Research and Treatment. 2007;106:S19-S.

28. Barbas AS, Mi J, Clary BM, White RR. Aptamer applications for targeted cancer therapy. Future oncology. 2010;6(7):1117-26.

29. Nimjee SM, Rusconi CP, Sullenger BA. Aptamers: an emerging class of therapeutics.

Annual review of medicine. 2005;56:555-83.

30. Proske D, Blank M, Buhmann R, Resch A. Aptamers--basic research, drug development, and clinical applications. Applied microbiology and biotechnology. 2005;69(4):367-74.

31. Carothers JM, Oestreich SC, Szostak JW. Aptamers selected for higher-affinity binding are not more specific for the target ligand. Journal of the American Chemical Society. 2006;128(24):7929-37.

32. Gold L, Polisky B, Uhlenbeck O, Yarus M. Diversity of oligonucleotide functions. Annual review of biochemistry. 1995;64:763-97.

33. Famulok M, Mayer G. Aptamers as tools in molecular biology and immunology. Current topics in microbiology and immunology. 1999;243:123-36.

34. Mayer G, Jenne A. Aptamers in research and drug development. BioDrugs : clinical immunotherapeutics, biopharmaceuticals and gene therapy. 2004;18(6):351-9.

35. Cerchia L, Hamm J, Libri D, Tavitian B, de Franciscis V. Nucleic acid aptamers in cancer medicine. FEBS letters. 2002;528(1-3):12-6.

36. Bates PJ, Laber DA, Miller DM, Thomas SD, Trent JO. Discovery and development of the G-rich oligonucleotide AS1411 as a novel treatment for cancer. Experimental and molecular pathology. 2009;86(3):151-64.

37. Ng EW, Shima DT, Calias P, Cunningham ET, Jr., Guyer DR, Adamis AP. Pegaptanib, a targeted anti-VEGF aptamer for ocular vascular disease. Nature reviews Drug discovery. 2006;5(2):123-32.

38. Li N, Nguyen HH, Byrom M, Ellington AD. Inhibition of cell proliferation by an anti-EGFR aptamer. PloS one. 2011;6(6):e20299.

39. Dastjerdi K, Tabar GH, Dehghani H, Haghparast A. Generation of an enriched pool of DNA

aptamers for an HER2-overexpressing cell line selected by Cell SELEX. Biotechnology and applied biochemistry. 2011;58(4):226-30.

40. Esposito CL, Passaro D, Longobardo I, Condorelli G, Marotta P, Affuso A, et al. A neutralizing RNA aptamer against EGFR causes selective apoptotic cell death. PloS one. 2011;6(9):e24071.

41. Kim MY, Jeong S. In vitro selection of RNA aptamer and specific targeting of ErbB2 in breast cancer cells. Nucleic acid therapeutics. 2011;21(3):173-8.

42. Chen CH, Chernis GA, Hoang VQ, Landgraf R. Inhibition of heregulin signaling by an aptamer that preferentially binds to the oligomeric form of human epidermal growth factor receptor-3. Proceedings of the National Academy of Sciences of the United States of America. 2003;100(16):9226-31.

43. Dassie JP, Liu XY, Thomas GS, Whitaker RM, Thiel KW, Stockdale KR, et al. Systemic administration of optimized aptamer-siRNA chimeras promotes regression of PSMA-expressing tumors. Nature biotechnology. 2009;27(9):839-49.

44. Watson SR, Chang YF, O'Connell D, Weigand L, Ringquist S, Parma DH. Anti-L-selectin aptamers: binding characteristics, pharmacokinetic parameters, and activity against an intravascular target in vivo. Antisense & nucleic acid drug development. 2000;10(2):63-75.

45. Guo J, Gao X, Su L, Xia H, Gu G, Pang Z, et al. Aptamer-functionalized PEG-PLGA nanoparticles for enhanced anti-glioma drug delivery. Biomaterials. 2011;32(31):8010-20.

46. Da Pieve C, Blackshaw E, Missailidis S, Perkins AC. PEGylation and biodistribution of an anti-MUC1 aptamer in MCF-7 tumor-bearing mice. Bioconjugate chemistry. 2012;23(7):1377-81.

47. Min K, Jo H, Song K, Cho M, Chun YS, Jon S, et al. Dual-aptamer-based delivery vehicle

of doxorubicin to both PSMA (+) and PSMA (-) prostate cancers. Biomaterials. 2011;32(8):2124-32.

48. Gradishar WJ. Albumin-bound paclitaxel: a next-generation taxane. Expert opinion on pharmacotherapy. 2006;7(8):1041-53.

49. Chen K, Xie J, Chen X. RGD-human serum albumin conjugates as efficient tumor targeting probes. Molecular imaging. 2009;8(2):65-73.

50. Wadas TJ, Wong EH, Weisman GR, Anderson CJ. Coordinating radiometals of copper, gallium, indium, yttrium, and zirconium for PET and SPECT imaging of disease. Chemical reviews. 2010;110(5):2858-902.

51. Blower PJ, Lewis JS, Zweit J. Copper radionuclides and radiopharmaceuticals in nuclear medicine. Nuclear medicine and biology. 1996;23(8):957-80.

52. Cai W, Wu Y, Chen K, Cao Q, Tice DA, Chen X. In vitro and in vivo characterization of ^{64}Cu-labeled Abegrin, a humanized monoclonal antibody against integrin alpha v beta 3. Cancer research. 2006;66(19):9673-81.

53. Niu G, Li Z, Xie J, Le QT, Chen X. PET of EGFR antibody distribution in head and neck squamous cell carcinoma models. Journal of nuclear medicine : official publication, Society of Nuclear Medicine. 2009;50(7):1116-23.

54. Prasanphanich AF, Nanda PK, Rold TL, Ma L, Lewis MR, Garrison JC, et al. [^{64}Cu-NOTA-8-Aoc-BBN(7-14)NH_2] targeting vector for positron-emission tomography imaging of gastrin-releasing peptide receptor-expressing tissues. Proceedings of the National Academy of Sciences of the United States of America. 2007;104(30):12462-7.

55. Liu Z, Li ZB, Cao Q, Liu S, Wang F, Chen X. Small-animal PET of tumors with (64)Cu-labeled RGD-bombesin heterodimer. Journal of nuclear medicine : official publication,

Society of Nuclear Medicine. 2009;50(7):1168-77.

56. Yang X, Hong H, Grailer JJ, Rowland IJ, Javadi A, Hurley SA, et al. cRGD-functionalized, DOX-conjugated, and (64)Cu-labeled superparamagnetic iron oxide nanoparticles for targeted anticancer drug delivery and PET/MR imaging. Biomaterials. 2011;32(17):4151-60.

57. Dearling JL, Voss SD, Dunning P, Snay E, Fahey F, Smith SV, et al. Imaging cancer using PET--the effect of the bifunctional chelator on the biodistribution of a (64)Cu-labeled antibody. Nuclear medicine and biology. 2011;38(1):29-38.

58. Anderson CJ, Dehdashti F, Cutler PD, Schwarz SW, Laforest R, Bass LA, et al. ^{64}Cu-TETA-octreotide as a PET imaging agent for patients with neuroendocrine tumors. Journal of nuclear medicine : official publication, Society of Nuclear Medicine. 2001;42(2):213-21.

59. Seo JW, Zhang H, Kukis DL, Meares CF, Ferrara KW. A novel method to label preformed liposomes with ^{64}Cu for positron emission tomography (PET) imaging. Bioconjugate chemistry. 2008;19(12):2577-84.

60. Garrison JC, Rold TL, Sieckman GL, Figueroa SD, Volkert WA, Jurisson SS, et al. In vivo evaluation and small-animal PET/CT of a prostate cancer mouse model using ^{64}Cu bombesin analogs: side-by-side comparison of the CB-TE2A and DOTA chelation systems. Journal of nuclear medicine : official publication, Society of Nuclear Medicine. 2007;48(8):1327-37.

61. Wadas TJ, Anderson CJ. Radiolabeling of TETA- and CB-TE2A-conjugated peptides with copper-64. Nature protocols. 2006;1(6):3062-8.

62. Huang CW, Li Z, Cai H, Shahinian T, Conti PS. Biological stability evaluation of the alpha2beta1 receptor imaging agents: diamsar and DOTA conjugated DGEA peptide. Bioconjugate chemistry. 2011;22(2):256-63.

63. Wei L, Ye Y, Wadas TJ, Lewis JS, Welch MJ, Achilefu S, et al. (64)Cu-labeled CB-TE2A

and diamsar-conjugated RGD peptide analogs for targeting angiogenesis: comparison of their biological activity. Nuclear medicine and biology. 2009;36(3):277-85.

64. Wadas TJ, Wong EH, Weisman GR, Anderson CJ. Copper chelation chemistry and its role in copper radiopharmaceuticals. Current pharmaceutical design. 2007;13(1):3-16.

65. Pieken WA, Olsen DB, Benseler F, Aurup H, Eckstein F. Kinetic characterization of ribonuclease-resistant 2'-modified hammerhead ribozymes. Science. 1991;253(5017):314-7.

66. Cummins LL, Owens SR, Risen LM, Lesnik EA, Freier SM, McGee D, et al. Characterization of fully 2'-modified oligoribonucleotide hetero- and homoduplex hybridization and nuclease sensitivity. Nucleic acids research. 1995;23(11):2019-24.

67. Kratz F. Albumin as a drug carrier: design of prodrugs, drug conjugates and nanoparticles. Journal of controlled release : official journal of the Controlled Release Society. 2008;132(3):171-83.

68. Kratz F. DOXO-EMCH (INNO-206): the first albumin-binding prodrug of doxorubicin to enter clinical trials. Expert opinion on investigational drugs. 2007;16(6):855-66.

69. Zhang Y, Hong H, Engle JW, Bean J, Yang Y, Leigh BR, et al. Positron emission tomography imaging of CD105 expression with a ^{64}Cu-labeled monoclonal antibody: NOTA is superior to DOTA. PloS one. 2011;6(12):e28005.

70. Petris MJ. The SLC31 (Ctr) copper transporter family. Pflugers Archiv : European journal of physiology. 2004;447(5):752-5.

71. Sefah K, Meng L, Lopez-Colon D, Jimenez E, Liu C, Tan W. DNA aptamers as molecular probes for colorectal cancer study. PloS one. 2010;5(12):e14269.

72. Yoshino I, Goedegebuure PS, Peoples GE, Parikh AS, DiMaio JM, Lyerly HK, et al. HER2/neu-derived peptides are shared antigens among human non-small cell lung cancer

and ovarian cancer. Cancer research. 1994;54(13):3387-90.

73. Brabender J, Danenberg KD, Metzger R, Schneider PM, Park J, Salonga D, et al. Epidermal growth factor receptor and HER2-neu mRNA expression in non-small cell lung cancer Is correlated with survival. Clinical cancer research : an official journal of the American Association for Cancer Research. 2001;7(7):1850-5.

74. Coombs LM, Pigott DA, Sweeney E, Proctor AJ, Eydmann ME, Parkinson C, et al. Amplification and over-expression of c-erbB-2 in transitional cell carcinoma of the urinary bladder. British journal of cancer. 1991;63(4):601-8.

75. Berchuck A, Kamel A, Whitaker R, Kerns B, Olt G, Kinney R, et al. Overexpression of HER-2/neu is associated with poor survival in advanced epithelial ovarian cancer. Cancer research. 1990;50(13):4087-91.

76. Gravalos C, Gomez-Martin C, Rivera F, Ales I, Queralt B, Marquez A, et al. Phase II study of trastuzumab and cisplatin as first-line therapy in patients with HER2-positive advanced gastric or gastroesophageal junction cancer. Clinical & translational oncology : official publication of the Federation of Spanish Oncology Societies and of the National Cancer Institute of Mexico. 2011;13(3):179-84.

77. Jorgensen JT. Targeted HER2 treatment in advanced gastric cancer. Oncology. 2010;78(1):26-33.

78. Cheng Z, De Jesus OP, Kramer DJ, De A, Webster JM, Gheysens O, et al. ^{64}Cu-labeled affibody molecules for imaging of HER2 expressing tumors. Molecular imaging and biology : MIB : the official publication of the Academy of Molecular Imaging. 2010;12(3):316-24.

79. Hoppmann S, Miao Z, Liu S, Liu H, Ren G, Bao A, et al. Radiolabeled affibody-albumin

bioconjugates for HER2-positive cancer targeting. Bioconjug Chem. 2011;22(3):413-21.

80. Ren G, Zhang R, Liu Z, Webster JM, Miao Z, Gambhir SS, et al. A 2-helix small protein labeled with ^{68}Ga for PET imaging of HER2 expression. Journal of nuclear medicine : official publication, Society of Nuclear Medicine. 2009;50(9):1492-9.

81. Tolmachev V, Nilsson FY, Widstrom C, Andersson K, Rosik D, Gedda L, et al. ^{111}In-benzyl-DTPA-ZHER2:342, an affibody-based conjugate for in vivo imaging of HER2 expression in malignant tumors. Journal of nuclear medicine : official publication, Society of Nuclear Medicine. 2006;47(5):846-53.

82. Delgado R, Sun YZ, Motekaitis RJ, Martell AE. Stabilities of Divalent and Trivalent Metal-Ion Complexes of Macrocyclic Triazatriacetic Acids. Inorg Chem. 1993;32(15):3320-6.

83. Clarke ET, Martell AE. Stabilities of the Alkaline-Earth and Divalent Transition-Metal Complexes of the Tetraazamacrocyclic Tetraacetic Acid Ligands. Inorg Chim Acta. 1991;190(1):27-36.

84. Boswell CA, Sun X, Niu W, Weisman GR, Wong EH, Rheingold AL, et al. Comparative in vivo stability of copper-64-labeled cross-bridged and conventional tetraazamacrocyclic complexes. Journal of medicinal chemistry. 2004;47(6):1465-74.

85. Hoppmann S, Qi S, Miao Z, Liu H, Jiang H, Cutler CS, et al. ^{177}Lu-DO3A-HSA-Z EGFR:1907: characterization as a potential radiopharmaceutical for radionuclide therapy of EGFR-expressing head and neck carcinomas. Journal of biological inorganic chemistry : JBIC : a publication of the Society of Biological Inorganic Chemistry. 2012;17(5):709-18.

86. Healy JM, Lewis SD, Kurz M, Boomer RM, Thompson KM, Wilson C, et al. Pharmacokinetics and biodistribution of novel aptamer compositions. Pharmaceutical research. 2004;21(12):2234-46.

87. de Smidt PC, Le Doan T, de Falco S, van Berkel TJ. Association of antisense oligonucleotides with lipoproteins prolongs the plasma half-life and modifies the tissue distribution. Nucleic acids research. 1991;19(17):4695-700.

국문초록

목적: 인간 상피세포 성장인자 수용체2(HER2)는 유방암의 지표물질로 알려져있다. 특히 HER2가 과발현된 환자들은 나쁜예후를 보이고 치료에도 저항성을 갖는다. 현재까지는 단일클론 항체인 허셉틴을 이용해 HER2 표적영상 및 치료에 많이 이용한다. 하지만 항체를 이용한 영상은 신호대 배경비가 좋지 않아 표적율이 떨어진다. 따라서 생체내에서 HER2의 발현을 영상으로 확인할 수 있는 새로운 표적제의 개발이 필요하다. 새로운 표적제로 알부민과 단일가닥의 핵산서열인 앱타머를 이용하여 영상용 표적제를 개발하였고, 이를 통해 세포수준과 생체내에서 HER2를 과발현하는 유방암을 표적화 할 수 있는지를 평가하였다.

실험방법: HER2를 표적화 할 수 있는 핵산서열을 셀렉스 방법을 통하여 선별하였고, 알부민을 접합해 사용하였다. FITC를 붙인 앱타머를 이용하여 공초점현미경으로 세포 표적영상을 확인하였다. 알부민을 접합할 때 구리-64의 킬레이터로 SCN-DOTA나 NOTA를 붙였고 SMCC를 연결체로 하여 앱타머를 접합하였다. 이 알부민-앱타머 접합체에 방사성구리-64를 표지하였고, 다공성컬럼인 PD-10으로 표지된 접합체를 분리해낸 후 그 표지 효율을 크로마토그래피 방법으로 확인하였다. 양전자단층촬영 기술로 접합체의 생체영상을 시간별로 확인 하였고, 각 조직을 적출하여 감마카운터로 정량화 하였다. 또한 종양 절편에서 자가 방사 기록법으로 영상을 얻고 공초점현미경으로 형광을 관찰하였다.

결과: FITC를 붙인 HER2 앱타머가 HER2 과발현세포 특이적으로 표적화 되었다. 앱타머에 갈륨-68 또는 알부민-앱타머 접합체에 구리-64를 표지하였을 때 95% 이상의 표지효율을 보였고, 세포내 섭취율을 비교하여보니 MDA-MB468에

비해 KPL4에서 최대 3배정도 높았다. 또한 IC50값은 경쟁자로 이용한 알부민-앱타머 접합체에서는 1.44 nM, NOTA-앱타머 접합체에서는 12.97 nM, 앱타머-비오틴 접합체에서는 9.68 nM 이었다. MDA-MB468과 KPL4 종양모델을 이용해 생체내 영상을 획득하였다. 갈륨-68 또는 구리-64를 표지한 앱타머의 경우 소변과 간경로를 통해 몸밖으로 빠르게 배설되었다. 하지만 양전자단층영상에서 알부민-앱타머 접합체는 소변으로 배설되는 것이 앱타머에 비해 적었고, KPL4 종양에 방사능 섭취증가가 시간이 지남에 따라 증가되었다. 또한 각각의 조직을 적출하여 감마카운터로 측정하였을 때에도 KPL4종양에 높게 축적되었다. 종양조직 절편을 자기방사법으로 촬영한 영상에서도 KPL4 종양에 높게 축적되었고, 알부민을 접합한 표적앱타머가 앱타머만을 이용한 것보다 더 많은 양이 종양내에 섭취 되었다. 이렇게 KPL4 종양내에 알부민-앱타머가 축적된 부분은 HER2가 발현하는 부분 일부에 일치하였다.

결론: 앱타머에 알부민을 접합하여 혈액내 머무르는 시간을 증가시킬 수 있었고, 효과적인 HER2 표적 영상을 얻을 수 있었다. 따라서 구리-64를 표지한 알부민-앱타머 접합체는 HER2의 효과적인 표적제로 사용할 수 있다.

핵심어: 인간 상피세포 수용체 2 (HER2), 앱타머, 알부민, 양전자 단층 촬영 영상, 구리-64, 표적치료

학번 : 2010-30593